homothorax is a modifier of radiation sensitivity in *Drosophila melanogaster bantam* mutants

Geoffrey Meyerhof
10 April 2017

Departmental Honors Thesis
Department of Molecular, Cellular, and Developmental Biology
College of Arts and Sciences
University of Colorado at Boulder

Thesis Advisor: Dr. Tin Tin Su
Department of Molecular, Cellular, and Developmental Biology
MCDB Honors Thesis Committee Member: Dr. Christy Fillman
Department of Molecular, Cellular, and Developmental Biology
Honors Thesis Committee Member: Dr. Rebecca Safran
Department of Ecology and Evolutionary Biology

Keywords: *bantam, homothorax, Drosophila melanogaster,* radiation, apoptosis, RNAi, cancer

Abstract

Radiation resistance in human cancers represents a massive impediment for successful tumor treatment. The fruit fly *Drosophila melanogaster* is an excellent model for human radiation resistance because of its largely conserved apoptotic pathways and malleable genome. This thesis investigates the genetic regulatory mechanisms for *bantam (ban),* an anti-apoptotic microRNA. To first identify genes that interact with *ban,* a forward genetic screen was conducted. This screen looked for genes that yielded radiation dependent pupal lethality in a *ban* deficient background. From this screen the transcription factor, *homothorax,* was identified as displaying radiation dependent synthetic lethality with *ban*. To investigate the mechanism of synthetic lethality, larval wing imaginal disc were examined. It was found that *hth* deficiency does not modify apoptosis in *ban* deficient wing disc. Nor does *hth* seem to play a direct role in *ban* activation. However, the inhibition of *hth* was shown to result in aberrant cell migration and exacerbate wing disc overgrowths following irradiation. Additionally, preliminary data indicates that *hth* plays a role in the radioprotective Mahakali Effect. Specifically, a reduction in *hth* is correlated with a reduction in radiation protection from apoptotic cells. Though a direct mechanistic link between *hth* and *ban* has yet to be identified, a plausible mechanism of induced radiation sensitivity has emerged. It is speculated that some combination of cell death (from *ban* dysfunction) and aberrant recovery (from *hth* dysfunction) results in the synthetic lethality observed in *ban/hth* pupa following irradiation.

Introduction

The goal of this research project was to investigate the genetic mechanisms employed by *Drosophila* to regulate expression of microRNA *bantam.* Loss of function mutations affecting *bantam* dramatically reduce *Drosophila's* ability to mitigate damage from genotoxic insults such as radiation. Working with *Drosophila* presents an opportunity to better understand how metazoan cells respond to radiation in a tissue and organ specific context. Given that fundamental cellular pathways regulating cell death are largely conserved across species, results from this research have potential relevance to mammalian systems. This is particularly germane to cancer, as malignant tumors are often characterized by radiation resistance.

Cancer and radiation resistance

In the United States, cancer is the second leading cause of death and is poised to surpass heart disease as the leading cause of mortality in the coming years. It is estimated that 50% of all American men and 33% of American women will at some point in their life develop a type of malignant tissue growth (Siegel et al. 2015). Cancer is a collection of diseases that are characterized by a population of cells that undergo unrestricted growth and division to form a tumor. Malignant tumors can invade surrounding tissues, which ultimately disrupts tissue/organ function. Cancer is a genetic disease and its onset is most commonly associated with mutations affecting the cell cycle (Chow 2010). Gain of function mutations that transform proto-oncogenes into oncogenes stimulate growth and division of the cell. Loss of function mutations affecting tumor suppressor genes inhibit cell cycle checkpoints, which normally serve to promote DNA repair and apoptosis. Together, oncogenes and tumor suppressor genes often act as the drivers for cancer (Vogelstein et al. 2013).

Cancer is primarily treated with some combination of surgery, radiation therapy, and/or drug treatment (Al-Lazikani et al. 2012). Radiation therapy and many drug treatments seek to eliminate cancer cells by damaging their DNA. Given a sufficient level of DNA damage, the cancer cell will undergo necrosis or apoptosis (Jackson and Bartek 2009). However, in order for this strategy to be effective cancerous tissues must be preferentially targeted. This is

accomplished by leveraging the differences between cancerous and non-cancerous cells. One major difference between these two cell types is their rate of cell division. Cancer cells divide more rapidly than healthy cells and are subsequently more likely to be replicating their DNA and undergoing mitosis (Brown and Wouters 1999). Because chromosomes are decondensed in the S phase of the cell cycle, they are particularly vulnerable to damage by radiation. With increased DNA damage comes an increased likelihood that that the cancer cell will apoptose as the result of the G1/S or G2/M cell-cycle checkpoint. These cell cycle checkpoints ensure that DNA has neither double strand breaks nor DNA crosslinking prior to DNA replication or mitosis (Pawlik and Keyomarsi 2004). If either of these DNA aberrations are present, the checkpoint kinases ATM or ATM can become phosphorylated. This results in a kinase cascade where Chk2/Chk1 and tumor suppressor genes (such as p53) are also phosphorylated. At this point, the cell cycle is stalled and DNA repair is attempted. If DNA repair is unsuccessful, the cell either undergoes apoptosis, becomes senescent, or propagates its mutations to subsequent generations of cells (Jackson and Bartek 2009).

Resistance to radiation is believed to cause treatment failure of ~90% of patients with metastatic cancer (Longley 2005). Unfortunately, loss of p53 function is the most common mutation found in human solid tumors (Levine and Oren 2009). Because p53 plays a crucial role in the radiation-induced apoptosis, mammalian cells lacking p53 are particularly radiation resistant (Lowe el al. 1993). Ultimately, there is significant clinical relevance in understanding the mechanisms of radiation resistance.

Drosophila as a model organism

The fruit fly, *Drosophila melanogaster,* is a versatile model organism that possesses a number of characteristics that lend it to being a model for human disease. Most notably, ~75% of genes identified in human disease have a functional homolog in *Drosophila.* Of these genes, ~85% of the proteins they encode have identical functional domains to their mammalian counterparts (Loyd and Taylor 2010). Additionally, *Drosophila's* simplified genome is amenable to genetic manipulation. However, unlike other simple model organism (such as *C. elegans*), *Drosophila* possesses a number of useful characteristics for mammalian comparison, including male/female sexes, a heart, brain, eyes, and p53-dependent radiation-induced cell death (Papatheodorou et al. 2014; Wichmann et al.

2006). Because of *Drosophila's* ~8.5 day lifecycle and ability to produce hundreds of offspring, complex mating schemes can be completed in a fraction of the time needed for murine models.

Drosophila exhibits complete metamorphosis. That is, it passes through an egg, larval (first, second, and third instar), and pupal stage prior to becoming an adult fly. Larvae contain precursors to adult fly organs known as "imaginal discs". These discs are formed from a continuous folded sheet of epithelial cells (Aldaz and Escudero 2010). Because imaginal discs contain tightly regulated patterns of genetic expression, can undergo substantial regeneration, and display cell polarity, they are a useful medium for studying cancer (Grzeschik et al. 2007). Notable contributions made to the field of cancer biology from *Drosophila* research include characterization of the tumor suppressor genes *p53*, *Rb*, and *APC* (Fan et al. 2009; Lee et. al. 2010) Additionally, growth-promoting pathways such as NOTCH and WNT (*Drosophila* wingless) are conserved in *Drosophila* and their perturbation leads to phenotypes that are observable in the wing discs (Simon et al. 2014; Huang et al. 2008).

Figure A: Larval wing disc

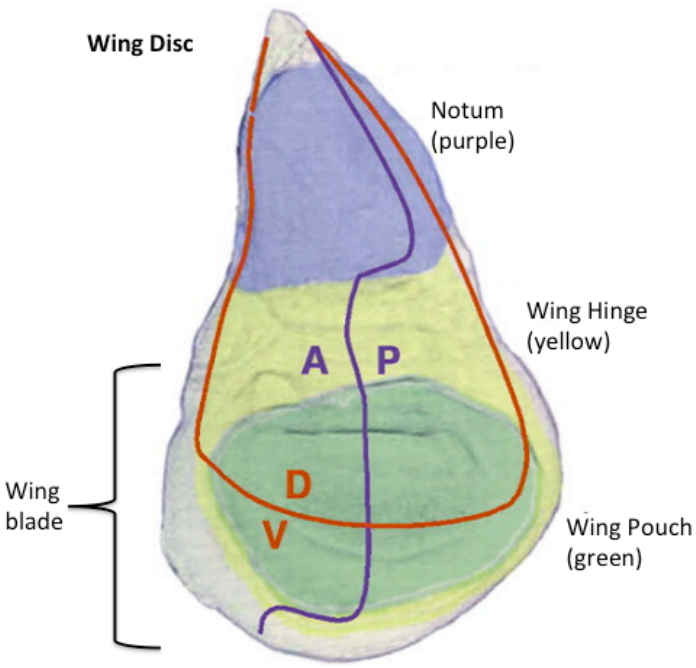

Figure A: ***A larval wing disc showing different regions and different compartment boundaries. Adapted from Butler et al. 2003.***

The following experiments described in this thesis utilize the *Drosophila* wing imaginal disc. The wing disc can be subdivided into several structures, which include the wing hinge, wing blade, and notum (illustrated in Fig. A). Additionally, the wing can be sectioned into the anterior/posterior, dorsal/ventral, and proximal/distal axes. Each axis and compartment of the wing imaginal disc has distinct genetic expression patterns. Expression of the transcription factor engrailed (*en)* is confined to the posterior compartment of the wing disc. En works to activate the morphogen, hedgehog (Hh), which

then emanates from the posterior compartment of the wing disc (Nahmad and Stathopoulos 2009). Conversely, the anterior compartment of the wing disc is characterized by the expression of patched (ptc) and the segment polarity transcription factor, cubitus interuptis (ci) (Johnson et al. 1995).

Figure B: *ptc* and *ci* expression in larval wing discs

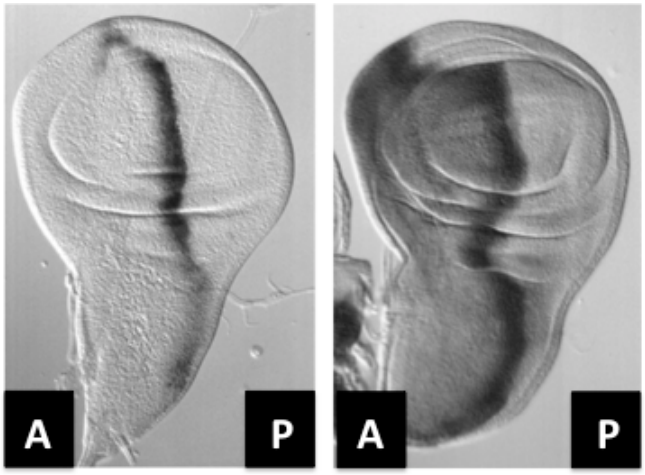

Figure B: ***Larval wing discs with LacZ reporter for ptc (left) and ci (right). 'A': anterior wing disc. 'P': posterior wing disc. Adapted from Johnson et al. 1995.***

The GAL4-*UAS* Expression System

The GAL4-*UAS* expression system allows for spatial and temporal regulation of gene expression in *Drosophila.* This system works by using the yeast transcription factor, GAL4, to activate genes downstream of an *upstream activating sequence* (*UAS)*. Specifically, flies can be engineered to contain a GAL4 transgene that is under the control of an active promoter. GAL4 then binds to the enhancer sequence, UAS, which has been engineered such

Figure C: GAL4-*UAS* Expression in *Drosophila*

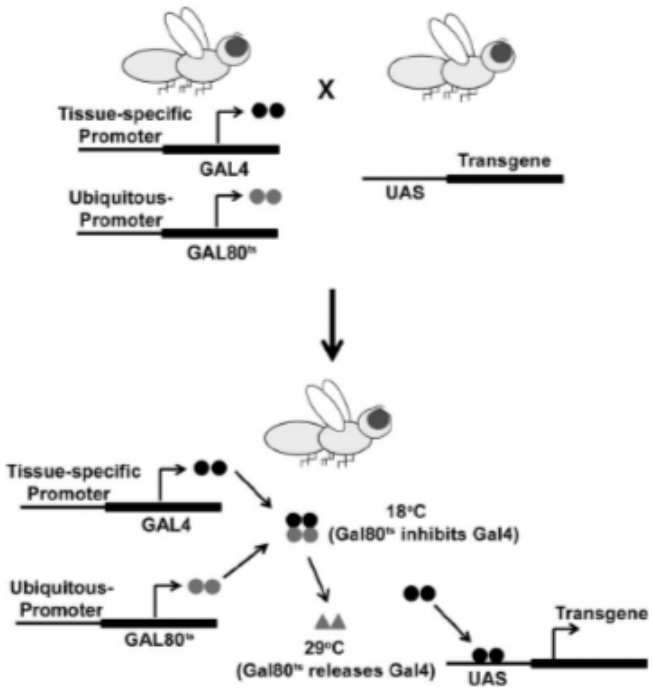

Figure C*: Schematic illustrating general protocol for GAL4-UAS expression. Note, flies need at least one copy of GAL4 to express genes under control of UAS sequence. Adapted from Wolf and Rockman 2011.*

that it is upstream from a gene of interest. *UAS* is transcriptionally inactive in the absence GAL4 (Duffy 2002). Tissue specificity can be selected for by expressing GAL4 from a tissue specific promoter (such as *en* or *ptc*). This powerful feature of the GAL4-*UAS* system allows for nuanced investigation of genetic expression. This is especially useful for investigating how cells behave in response to a unique microenvironment. Temporal specificity can be achieved by expressing the temperature sensitive GAL4 repressor, GAL80, from a ubiquitous promoter. Subsequently, moving flies from a temperature restrictive to a temperature permissive environment (i.e. 18°C [inactive] to 29°C [active]) results in the expression of a gene of interest under GAL4-*UAS* control. This regulation is crucial for expressing genes whose constitutive expression would result in embryonic lethality (Wolf and Rockman 2011).

RNA interference and microRNAs

RNA interference (RNAi) refers to a phenomenon in which small non-coding RNA molecules post-transcriptionally silence gene expression. These 20-23nt RNAs were first characterized in *C. elegans* where they were identified as having a role in developmental timing (Lee et al. 1993). RNAi's have since been shown to be present in mammalian cells where they are involved in a variety of processes, including progression and suppression of the cell cycle (Calin and Croce 2006). There are several classes of RNAi, which include small interfering RNA (siRNA), micro RNA (miRNA), and piwi-interacting RNA (piRNA). These interfering RNAs all post-transcriptionally repress gene expression and generally follow a

Figure D: ***miRNA biogenesis***

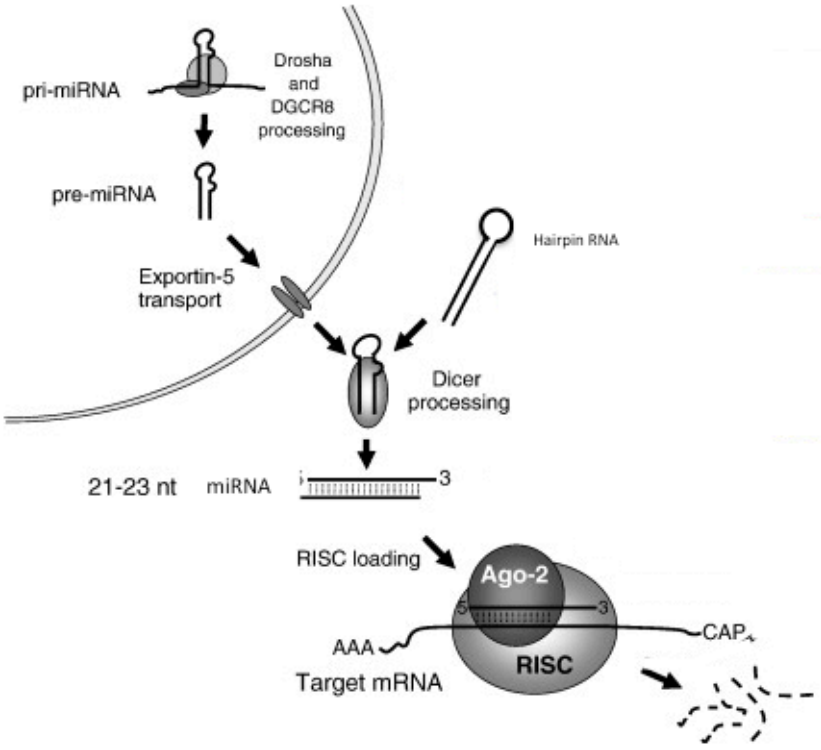

Figure D: ***Diagram of miRNA pathway. miRNA transcript is modified by Drosha (in nucleus) and Dicer (in cytoplasm) before it can associate with RISC complex and degrade target mRNA. Adapted from Aagaard and Rossi 2007.***

similar pathway of biogenesis. Their primary differences are with regards to pre-RNAi processing, length, and mRNA specificity (Lam et al. 2015). For example, miRNAs are only partially complementary to their 3'-UTR mRNA target, while siRNAs are fully complementary to their target mRNA (Bartel 2009). Interfering RNAs are initially transcribed in the nucleus as long primary transcripts. In the case of miRNA, this primary transcript (pri-miRNA) is cleaved by the nuclease, Drosha, to form a hairpin pre-miRNA. This hairpin structure then exits the nucleus where it is further cleaved by the enzyme Dicer. Finally, this mature miRNA is loaded onto the RNA-induced silencing complex (RISC) where it can degrade its target mRNAs (Lam et al. 2015).

miRNA *bantam* and apoptosis in *Drosophila*

The *Drosophila* gene, *bantam* (*ban*), encodes a 21nt miRNA. *ban* was first identified in a screen for genes that when overexpressed, resulted in overgrowths of the imaginal discs. It was observed that *ban* overexpression resulted in an increased number of normal sized cells. Conversely, *ban* loss of function was observed to result in a reduced number of normal sized cells and smaller imaginal discs (Hipfner et al. 2002). *ban* targets the 3'-UTR of mRNA from the pro-apoptotic gene, *head involution defective* (*hid*). In addition to its anti-apoptotic role, *ban* also promotes cell proliferation via the Hippo tumor suppressor pathway (Brenecke et al. 2003; Peng et al. 2009).

As in mammals, apoptosis in *Drosophila* is characterized by a cascading activation of cysteine-aspartate proteases, aptly named "caspases". Caspase zymogens can be activated via intrinsic and extrinsic cellular pathways (Shklover et al. 2015). However, the terminal step in both pathways is the activation of effector caspases (e.g. DCP-1, a caspase-3 homolog). Activated effector caspases have over 65 substrates, however,

Figure E: Apoptosis in Drosophila

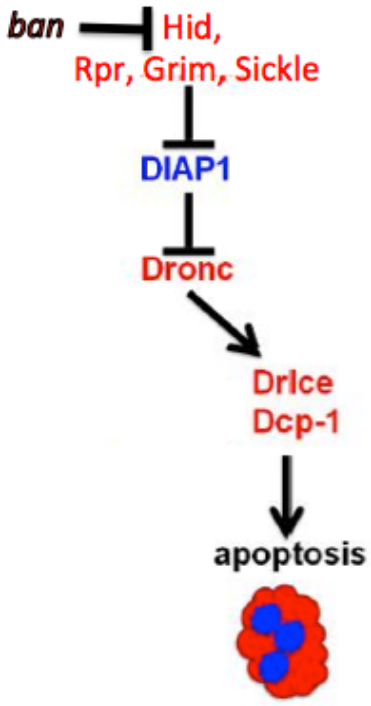

Figure E. ***apoptotic pathway in Drosophila. Pro-apoptotic proteins Hid, Rpr, Grim, and Sickle inhibit the inhibitor of apoptosis, DIAP1. This allows for the initiator caspase, Donc, to activate the effector caspases DCP-1 and DRICE. Note, ban targets hid mRNA. Adapted from Su 2015.***

they generally inactivate pro-mitotic proteins and activate pro-apoptotic proteins (Kornbluth and White 2005). Subsequently, apoptosis is often regulated at the level of caspase activation. One such regulatory mechanism comes from the *Drosophila* inhibitor of apoptosis protein 1 (DIAP1). DIAP1 inhibits apoptosis activation through sequestration and ubiquitin-mediated degradation of initiator caspases (Salvesen and Duckett 2002). Conversely, the pro-apoptotic proteins Reaper, Sickle, Grim, and Hid (SMAC/DIABLO homologs) bind to and inhibit DIAP1 (Bilak and Su 2009). These pro-apoptotic proteins can be activated by a variety of signals including radiation induced DNA damage, steroid hormones, developmental signals, and heat stress (Steller 2008).

The Mahakali Effect and *bantam*

When cells in *Drosophila* wing imaginal discs are killed, dying cells protect their neighbors from apoptosis. This phenomenon has been named the "Mahakali Effect", after the Hindu Goddess of death who protects her followers (Bilak et al. 2014). This effect is observable when cells are killed by a variety of means and results in a protective zone spanning ~100mm. It is hypothesized that dying cells release PVF1, which binds to the receptor Tie and ultimately leads to *ban* activation in cells neighboring apoptotic cells. Genetic removal of *tie*, *pvf1*, or *ban* reduces the protective effect from dying cells. In this thesis, the Mahakali Effect is experimentally induced by using a GAL4-*UAS* system to drive the expression of *dE2F1-RNAi* from a *ptc* promoter. *dE2F1* is a pro-mitotic gene and its inhibition via *ptc* results in a stripe of apoptotic cells along the anterior-posterior boundary (Fig. B and Fig. 5). If larvae are then irradiated after cells have been killed by *ptc>dE2F1*$^{\text{RNAi}}$, a protective effect can be observed. For unknown reasons, this protective effect is most pronounced on the anterior side of the wing pouch (Bilak et al. 2014).

***Homothorax* and larval development**

The expression of *hox* genes in both vertebrates and invertebrates is tightly regulated and often requires the presence of cofactors to achieve adequate DNA binding specificity. One such cofactor is *homothorax (hth).* Together with an additional cofactor, extradenticle (Exd), Hth can bind with various Hox proteins to form a complex. In the nucleus this complex acts to ensure proper Hox DNA specificity (Ryoo et al. 1999). In the wing disc, it has been observed that *hth*

acts as a positive regulator of growth in the wing notum and wing hinge. Knockdown of *hth* in the wing results in a reduction in the size of the notum and hinge. Hth elicits its proliferative effects within the wing notum/hinge via JAK/STAT signaling. Ectopic expression of *hth* in the wing pouch results in JAK/STAT dependent wing pouch overgrowths. However, down-regulation of JAK/STAT signaling is required for wing blade development. Subsequently, the elimination of *hth* results in an overgrowth of the wing blade (Ayala-Camargo et al. 2013). In the eye disc, *hth* expression is initiated in eye progenitor cells via Wg signaling. Once *hth* expression is activated in the eye disc, Hth can complex with the protein, teashirt (tsh). The binding of hth to tsh inhibits the Hippo tumor suppressor pathway, allowing for differentiation and proliferation of the eye progenitor cell population. Notably, this proliferation is dependent upon the induction of *ban* (Peng et al. 2009).

Homothorax, MEIS1, and Leukemia

Much like in *Drosophila,* the mammalian *hth* homolog, *meis1,* binds to the *exd* homolog, *pbx* to direct the expression of *hox* genes, most notably *hoxa9* (Bonnet and Dick 1997). The expression of *meis1* has been best studied with regard to hematopoietic stem cell (HSC) transformation. Specifically, the association of Hoxa9 with Meis1 allows for transformation of HSCs to B-lymphocytes, natural killer cells, and T-lymphocytes (Kroon et al. 1998). *meis1* and *hoxa9* were first identified as being relevant to cancer when it was shown that their overexpression led to the onset of leukemia in mice (Kroon 1998). Subsequent biopsies from human tumors have indicated a conserved role for these genes in human blood cancers. The aberrant expression of the Hoxa9-Meis1 protein complex has been associated with acute myeloid leukemia, lymphoblastic leukemia, and mixed lineage leukemia (Faber et al. 2009). Though each of these leukemias differs in its mechanism of induction, they all result in increased expression *hoxa9*. The best-characterized leukemogenic mechanism is in acute myeloid leukemiac (AML). AML is characterized by the genetic fusion of *hoxa9* to the nucleoporin gene, *nup98,* such to remove the regulatory region of *nup98.* This results in constitutive *hoxa9* expression (Kroon 1998). However, in both mice and human tumor cell lines, the constitutive expression of just *hoxa9* does not result in malignant cell proliferation. Like in *Drosophila*, Hoxa9 requires a cofactor for adequate DNA binding. Predictably, a *hoxa9-nup98* mutation is most virulent when it exists in a genetic background that is concurrently overexpressing *meis1* (Krivstov 2006). It is

believed that the binding of HOXA9-NUP98 to Meis1 not only serves to amplify gene expression via DNA binding but also serves to inhibit cell death by preventing Meis1 mediated apoptosis (Faber 2009). It has been shown that activated Hoxa9 has ~1,000 transcriptional targets and that Hoxa9 also plays a role silencing the transcription of several hundred genes. The breadth of genes that respond to Hoxa9 have shrouded the precise mechanism by which its transcriptional activation contributes to leukemia. However, it has been observed that Hoxa9 expression generally up-regulates proliferative genes (Collins and Hess 2016).

Here it is shown that *homothorax* interacts with *bantam* to sensitize larvae to IR. The mechanism of lethality yielded by these two genes has yet to be determined. *hth* does not modify apoptosis in *bantam* deficient wing discs. Nor has *hth* been found to be radiation sensitive on its own. However, the absence of *hth* has been found to exacerbate wing disc overgrowths following radiation. Additionally, preliminary data indicates that *hth* attenuates the radioprotective "Mahakali Effect". Given *bantam's* known ability to mitigate cell death following apoptosis, it is hypothesized that a combination of cell death and aberrant regeneration is responsible for *bantam/homothorax* synthetic lethality.

Methods

Fly Husbandry for Genetic Screen

Virgin wild type flies were crossed to chromosomally deficient flies (*df)* and flies harboring a bantam (*ban*) mutation. Heterozygous stocks were maintained over s TM6 "tubby" (Tb) tagged balancer chromosome. Presence of Tb phenotype was used to assess genotype of pupa. Flies were allowed to mate for three days prior to embryo collection. Embryos were collected for 8 or 24h (as indicated) in uniform plastic vials containing a uniform volume of food. This ensured that larvae in different vials received a nearly uniform dose of radiation. Four days after the end of embryo collection, third instar larvae were irradiated with 8000R of x-ray radiation. Pupal eclosion (i.e. the emergence of an adult fly from its pupal case) was quantified ten days after irradiation. Flies/larvae were kept at 25°C for the duration of the experiment.

Chi-Square Test

A chi-square test was used to quantify how significantly the experimentally observed rates of eclosion differed from the expected values. Rates of eclosion from *ban/df* pupae were compared to rates of eclosion from *ban/+* and *df/+* pupae. Degrees of freedom = 1. Statistical significance set at $p<0.001$ (critical value 10.827). The following table and equations were used to generate chi-square values:

ban/+	***df/+***		***ban/df***			***Chi-Square Test***						
Pupal Eclosion	**Pupal Eclosion**	**Expected Pupal Survival**	**Pupal Death**	**Total Pupae**	**Pupal Eclosion**	**Expected Pupal Survival**	**Observed Pupal Survival**	**X^2_{Live}**	**Expected Pupal Death**	**Observed Pupal Death**	**X^2_{Die}**	**X^2_{Sum}**

Equations for Chi-Square Value:

- $Pupal\ Eclosion = \frac{Eclosed\ Pupa}{Total\ Pupa}$
- $Expected\ Pupal\ Survival_{Df/+} = (\%Eclosion_{Df/+}) * (\%Eclosion_{ban/+})$
- $Expected\ Pupal\ Survival_{X^2} = (Total_{ban/Df}) * (Expected\ Survial_{Df/+})$
- $X^2_{Live} = \frac{(Observed_{Lived} - Expected_{Lived})^2}{Expected_{Lived}}$
- $Expected\ Pupal\ Death = (Total_{ban/Df}) * (1 - Expected\ Survial_{Df/+})$
- $X^2_{Die} = \frac{(Observed_{Died} - Expected_{Died})^2}{Expected_{Died}}$
- $X^2_{Sum} = X^2_{Live} + X^2_{Die}$

Irradiation

Larvae were irradiated in food in a Faxitron Cabinet X-ray System Model RX- 650 at 115 kV and 5.33 rad/sec. Larvae received either a dose of 4000R or 8000R (12'30" and 25' respectively), which induced an intermediate level of lethality. Irradiated larvae were incubated for indicated amount of time before dissection.

Larvae Dissection and Staining

Wing discs imaged for GFP intensity were removed from larvae in phosphate buffered saline (PBS) and mounted in between glass slide and coverslip for "live imaging". Wing discs imaged for caspase staining were removed from larvae that had been dissected in PBS and then fixed in 4% para-formaldehyde for 30'. Samples were then washed in PBS and permeabalized for 5' in 0.5% Triton-X. Triton-X was diluted in PBS. Prior to the application of primary antibody,

samples were blocked in normal goat serum (NGS) for 1-2h in order to prevent non-specific antibody binding. Samples were left in primary antibody for ~8-12h and then washed three times in 0.01% Triton-X. Samples were then stained with 1:1000 dilution of Hochest DNA Stain and again washed in 0.01% Triton-X. Samples were then placed in secondary antibody for 2h. After completion of secondary antibody incubation, samples were again washed 3 times in 0.01% Triton-X. Samples were mounted on a glass slide in Flouromount G (Southern Biotech). Primary antibodies were diluted in NGS as follows: Rabbit anti DCP1 1:100, Rat anti Engrailed 1:300. Both secondary antibodies were diluted 1:200 in NGS.

Image Quantification

Images were captured on a Nikon inverted fluorescence microscope with a Hamamatsu image EM C9 100–13 EM CCD camera and processed using ImageJ software. Fluorescence intensity was quantified by examining the mean pixel value from ImageJ. All fluorescence intensities were normalized to their background intensity. Images that are directly compared were processed identically.

Fly Stocks/Genotypes

	Bloomington Stock #	Genotype	Allele Behavior	Reference
bantam	10154	[1] w[1118]; P{w[+mC]=lacW}ban[L1170a], l(3)L1170b[L1170b]/TM3, Ser[1], To be called: *ban*^{1170}	hypomorph	Brennecke et al. 2003
	58878	w[*]; Df(3L)ban[Delta1]/TM3, P{w[+mC]=GAL4-twi.G}2.3, P{UAS-2xEGFP}AH2.3, Sb[1] Ser[1] to be called *ban* $^{\Delta 1}$	null	Hipfner et al. 2002
homothorax	11670	P{ry[+t7.2]=PZ}hth[05745] ry[506]/TM3, ry[RK] Sb[1] Ser[1] to be called, *hth*^{05745}	hypomorph	Rieckhoff et al. 1997
	7637	w[1118]; Df(3R)Exel6158, P{w[+mC]=XP-U}Exel6158/TM6B, Tb[1], to be called *hth*^{7637}	null	Corsetti et al. 2013
***UAS*-RNAi Stocks**	27655	y[1] v[1]; P{y[+t7.7] v[+t1.8]=TRiP.JF02733}attP2/TM 3, Sb[1] to be called X2-*hth*^{RNAi}	siRNA	-
	34637	y[1] sc[*] v[1]; P{y[+t7.7] v[+t1.8]=TRiP.HMS01112}attP2 to be called X3-*hth*^{RNAi}	siRNA	-
	-	*ptc*>GAL4;UAS-dsRNA against *dE2F1* to be called, *PE3*	RNAi	Morris et al. 2008
Other	-	*P{Tub-EGFP.ban}* on Chr II, to be called 20.X	Sensor	Brennecke et al. 2003
	5072	w[*]; P{w[+mC]=UAS-p35.H}BH1 to be called *UAS*-p35	UAS-transgene	Wells et al. 2006
	3605	W[1118], to be called w^{1118}	wild type	Kyrchanova et al. 2002

Balancer Chromosomes and Tags

- *Tb:* "Tubby" larval phenotype
- *TM6B*: Third multiple six balancer chromosome, *Tb* tagged (Craymer 1984)
- *Cy:* "Curly" adult wing phenotype
- *CyO-GFP:* "Curly Oster" balancer chromosome, *Cy* and *GFP* tagged (Casso et al. 1999)

Results

Hth was identified in a screen for modifiers of eclosion after irradiation in *ban* mutants

In order to identify genetic candidates involved in *ban's* anti-apoptotic mechanism in *Drosophila*, a forward genetic screen was conducted to search for *ban* phenotypic modifiers. Flies harboring a hypomorphic *ban* allele (henceforth referred to as ban^{1170}) were crossed to flies with a chromosomal deficiency (Df). Four days after the start of embryo collection, larval progeny were exposed to an 8000R dose of ionizing x-ray radiation (IR). This dose was chosen as it resulted in an intermediate amount pupal death (~25%) and subsequently allowed for the screening of modifiers of radiation sensitivity. Ten days after exposure to IR, rates of pupal elcosion were quantified. (Fig.1A). Data were collected for various deficiencies that together spanned the entirety of the third chromosome (Fig. S3). For the purpose of this study, gene combinations that synergistically modified the *ban* phenotype (i.e. greater than additive pupal lethality after exposure to IR) were considered as candidates for modifiers of *ban* expression. Statistical significance of synergistic lethality was determined via chi-square test. (Fig.1B).

Figure 1A: Schematic of forward genetic screen

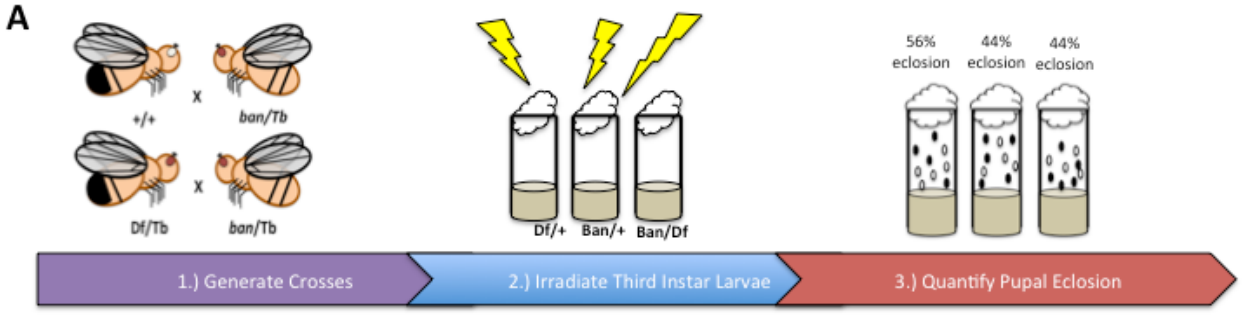

Figure 1A: ***shows a schematic of the forward genetic screen. Wild-type flies (+) were crossed to chromosomally deficient (Df) flies and flies harboring a bantam (ban) mutation. Heterozygous stocks were maintained over TM6 "tubby" (Tb) tagged balancer chromosome.***

Figure 1B: ***Chi-square test overview***

Figure 1B: A chi-square test was used to assess statistical significance of pupal lethality resulting from chromosomal deficiencies in ban deficient genetic background. Allelic combinations that resulted in greater than additive pupal lethality (i.e. ban/Df %eclosion < ban/+ %eclosion x Df/+ %eclosion) were deemed to have genetic interaction. See methods for complete explanation of chi-square analysis.

Hth [(I)305745, henceforth referred to as *hth*^{05745}] was identified as a modifier of pupal eclosion in *ban*^{1170} mutants. Pupa heterozygous for *hth*^{05745} and *ban*^{1170} had 23% eclosion (s.d. ± 14%). Pupa heterozygous for just *hth*^{05745} had 72% eclosion (s.d. ± 12%) and pupa heterozygous for just *ban*^{1170} had 70% eclosion (s.d. ± 17%). Chi-square analysis indicated that *ban*^{1170}/*hth*^{05745} pupa showed synergistic lethality after exposure to IR ($p<0.001$). To confirm these results, an additional *hth* and *ban* allele were tested for synthetic lethality. *hth*^{7637} [DF(3R)Exel6158] was also crossed to *ban*^{1170} and their pupal progeny had 40% eclosion (s.d. ± 10%) after exposure to IR. In contrast, *hth*^{7637} heterozygotes had 80% eclosion after exposure to IR. Chi-square analysis again indicated synergistic lethality for *ban*^{1170}/*hth*^{7637} pupa ($p<0.001$). *hth*^{05745}/*ban*^{1170} larvae not exposed to IR failed to show synergistic lethality when compared to their respective controls ($p>0.05$) (Fig. 1C). Lastly, flies harboring a deletion for *ban* (*ban*$^{\Delta 1}$) were crossed to *hth*^{05745} flies. The larval progeny from this cross failed to pupate after irradiation. However, un-irradiated *ban*$^{\Delta 1}$/*hth*^{05745} larvae did pupate and displayed 75% eclosion (s.d. ± 23%).

Figure 1C: ***Percent eclosion of hth/ban pupa***

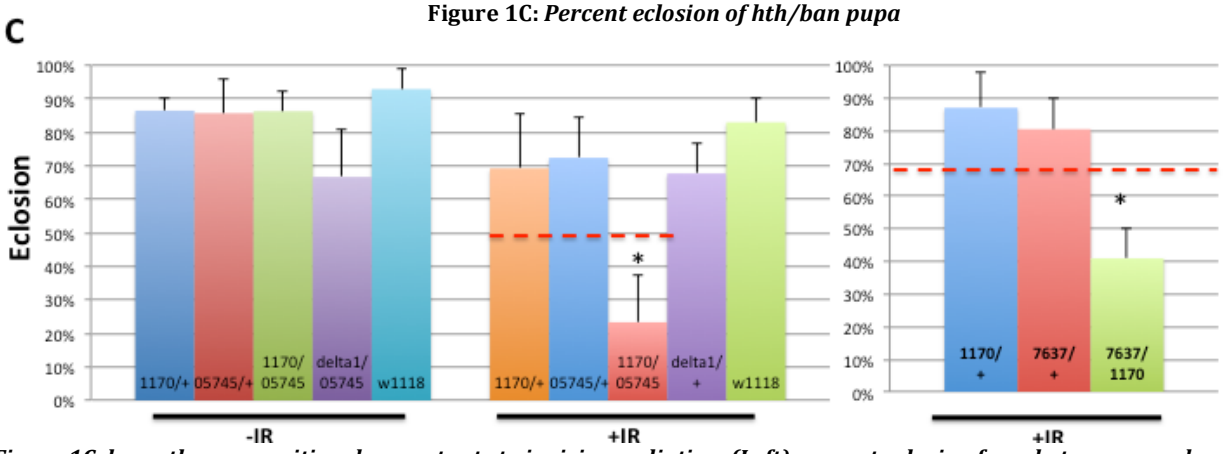

Figure 1C: homothorax sensitizes ban mutants to ionizing radiation. (Left) percent eclosion from heterozygous ban^{1170} (1170/+) pupa, heterozygous hth^{05745} (05745/+) pupa, doubly heterozygous (1170/+, 05745/+) pupa, and wild-type (w1118) pupa. (Right) percent eclosion from heterozygous ban1170 (1170/+) pupa, heterozygous hth^{7637} (7637/+) pupa, and doubly heterozygous pupa (1170/+,7637/+). Red dashed line indicates additive lethality (50% left and 69% right). Asterisk (*) indicates statistical significance corresponding to p<0.001.N=39-652 pupa from at least two independent experiments.

Hth does not modify apoptosis in ban/+ wing disc

Because of *ban's* anti-apoptotic role following exposure to IR, a plausible explanation for the observed synthetic lethality was an increase in apoptosis (Bilak et al. 2014 and Jaklevic et al. 2008). To test this hypothesis, third instar larvae were exposed to x-ray radiation and their wing imaginal discs were fluorescently labeled with an antibody against *Drosophila* cleaved executioner caspase (DCP-1). Apoptosis was scored by calculating the ratio between the area of the DCP-1 stain and the total area of the wing disc. The fractional area of DCP-1 stain in the wing disc of flies heterozygous for both hth^{7637} and ban^{1170} (*7637/1170)* was 0.16 (s.d. ± 0.06), while the fractional area for flies heterozygous for hth^{7637} (*7637/+)* was 0.10 (s.d. ± 0.05), and 0.12 for flies heterozygous for ban^{1170} (*1170/+)* (s.d. ± 0.02). Comparing these values revealed that *ban/hth* flies failed to show greater than additive apoptosis when compared to the sum of their respective controls (Fig. 2B). Subsequently, it is unlikely that apoptosis alone is responsible for the synthetic lethality observed in the genetic screen.

Figure 2A: ***Larval wing discs stained for apoptosis***

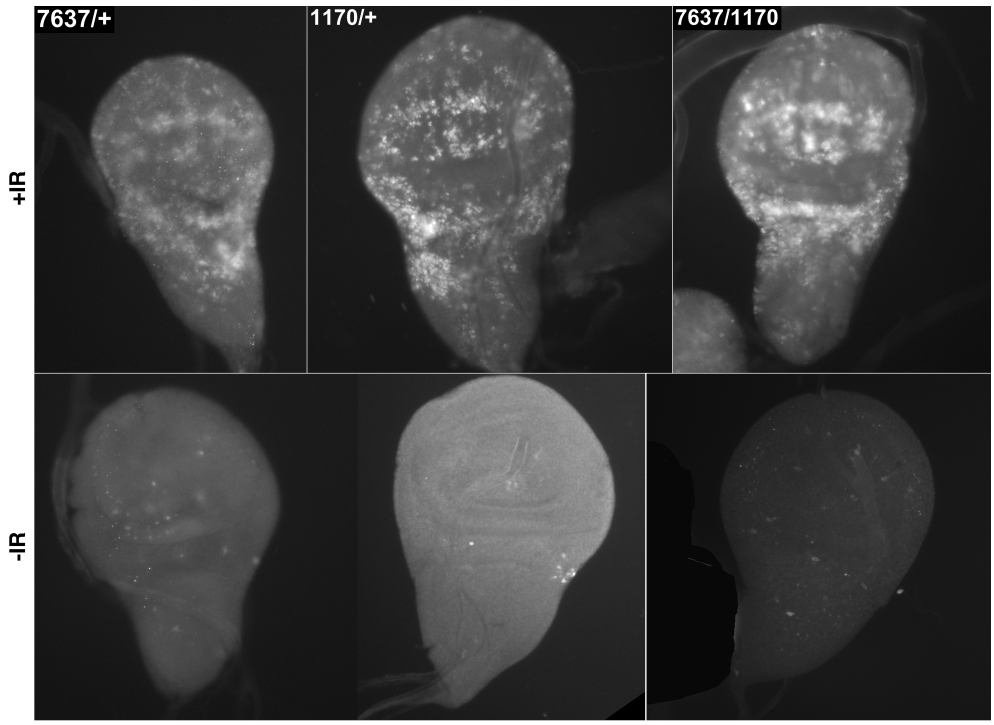

Figure 2A: Wing discs from third instar larvae are fluorescently labeled for apoptosis. Discs are labeled with fluorescently tagged antibody against Drosophila executioner caspase, DCP-1.

Figure 2B: ***Apoptosis in wing disc after IR***

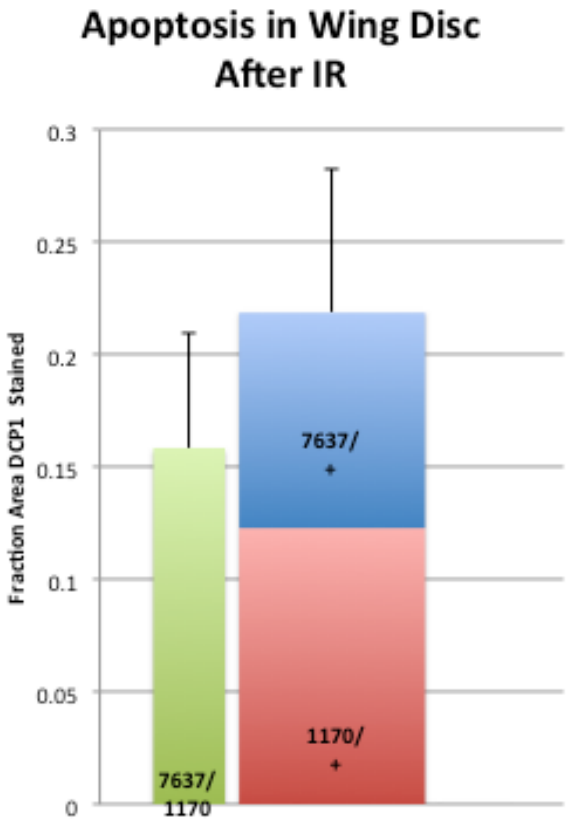

Figure 2B: Quantification of Fig. 2A. Graph displays fractional area of DCP-1 stain in wing disc 4h after exposure to 8000R of ionizing radiation. Note, apoptosis in ban/+ discs is not significantly affected by hth. Fractional area of DCP-1 stain was calculated by dividing the area of the stain by the area of the wing disc. N=6-11 wing discs per genotype from at least two separate experiments.

Figure 2C: Experimental timeline

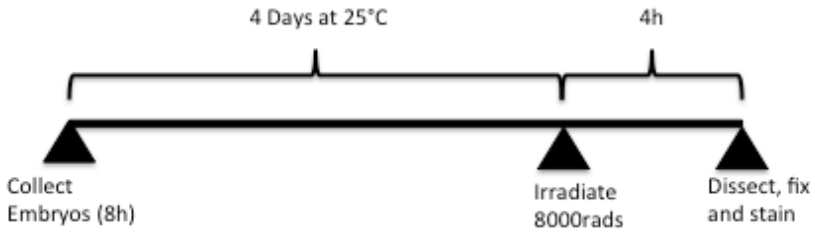

Figure 2C: Experimental timeline. Embryos were collected for 8h at 25°C . Four days after collection, third instar larvae were irradiated with 8000R of radiation. Four hours after irradiation, larvae were dissected, fixed, and stained for apoptosis

Hth does not affect *ban* sensor ± radiation

Homothorax (Hth) has been shown to act in conjunction with Teashirt (Tsh) to regulate *ban* expression in the *Drosophila* eye imaginal disc (Peng et al. 2009). However, prior to this investigation it was unknown whether a similar regulatory mechanism exists in the wing imaginal disc. In order to determine how *hth* affects *ban* activity in the wing disc, enhanced green fluorescent protein (EGFP) expression from a transgenic *"ban* sensor" (20.X) was monitored. This published *ban* sensor expresses EGFP from a ubiquitously active tubulin promoter and contains two perfect *ban* target sequences in its 3'-UTR. Subsequently, the expression of EGFP is inversely related to the activity of *ban* (Brennecke et al. 2003).

Two lines of evidence were generated to test whether hth has regulatory role for *ban* in the wing disc. First, *ban* sensor EGFP expression was measured in wing discs from third instar larvae 24h after exposure to 4000R of IR. Given that the half-life of GFP is ~26h, radiation induced changes in *ban* sensor EGFP are not readily observable until at least 24h after irradiation (Corish and Tyler-Smith 1999 and Jaklevic et al. 2008). Consistent with past findings, EGFP expression was reduced in irradiated wing discs, indicating an increase in *ban* activity (Fig. 3) (Jaklevic et al. 2008 and Bilak et al. 2014). *hth*^{05745} heterozygotes (*05745*/+) also showed a reduction in EGFP expression following irradiation, thus indicating that the hypomorphic *hth*^{05745} allele does not affect *ban* activity. EGFP expression was not significantly reduced in *ban*^{1170} heterozygotes following irradiation (Fig. 3A quantified in 3C). This allowed the allele to serve as a negative control.

Figure 3A: ***hth fails to modify ban sensor +/- radiation***

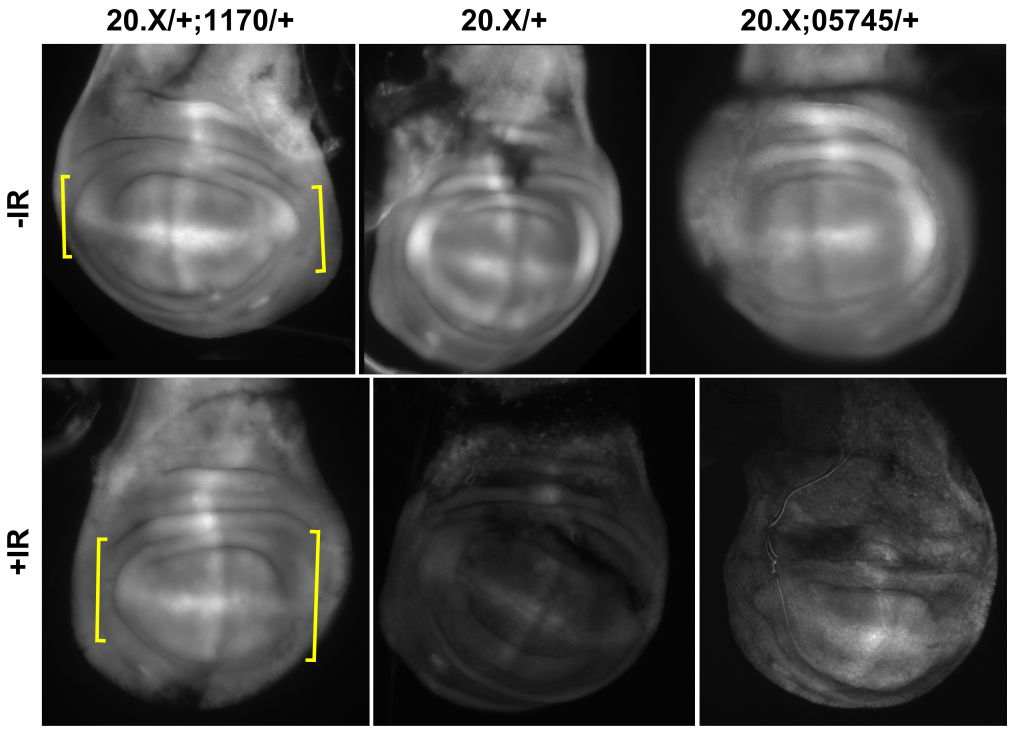

Figure 4A: Hth fails to modify ban expression. Heterozygous ban sensor (20.X/+) third instar larvae were exposed to 4000R of ionizing radiation. ban sensor EGFP intensity is inversely related to ban expression. Note change in EGFP expression in wing pouch (indicated via yellow brackets) among groups. Images were processed identically for direct comparison of fluorescence.

In order to address the possibility that the mutant *hth*^{05745} allele retains its *ban* regulatory function, *hth* was also post-transcriptionally repressed via RNAi in a *ban* sensor background. This was accomplished by using an *engrailed*>GAL4-*UAS* system to drive the expression of *hth*^{RNAi}. Because GAL4 was expressed from an *engrailed* promoter, there was targeted repression of *hth* in just the posterior compartment of the wing disc. Subsequently, the anterior compartment of the wing disc served as an internal control for changes in *ban* sensor expression. Because flies were also heterozygous for the temperature sensitive GAL4 repressor, GAL80, there was temporal regulation of *hth* knockdown. This was crucial as it was found that prolonged expression of *hth*^{RNAi} was embryonically lethal (data not shown). GAL4 was de-repressed in larvae from first to third instar (72h). Third instar larvae were then irradiated with 4000R of IR. Wing discs were removed 24h after irradiation to monitor EGFP expression. A uniform reduction in EGFP was observed from two distinct *hth*^{RNAi} lines (X2 and X3) (Fig. 3 e-h). Larvae expressing the viral anti-apoptotic protein, p35, were included as a positive control for change in EGFP expression (Mehrabadi et al. 2015). The inhibition of apoptosis via p35 reduced *ban* activity following exposure to IR. This is observable as the retention of EGFP in the anterior compartment of the wing disc, opposite to where p35 was expressed (Fig. 3B a-b). This p35 behavior is in contrast to what has been previously observed (Jaklevic et al. 2008). Previously, p35 expression has resulted in the retention of EGFP in the same compartment of its expression (Jaklevic et al. 2008; Bilak et al. 2014). The reason for this discrepancy is unknown. Given that EGFP expression from the *ban* sensor was changed regardless of *hth* status, it is unlikely that hth has a regulatory role for *ban* expression in the wing imaginal disc.

Figure 3B: ***hth^{RNAi} fails to modify ban sensor after IR***

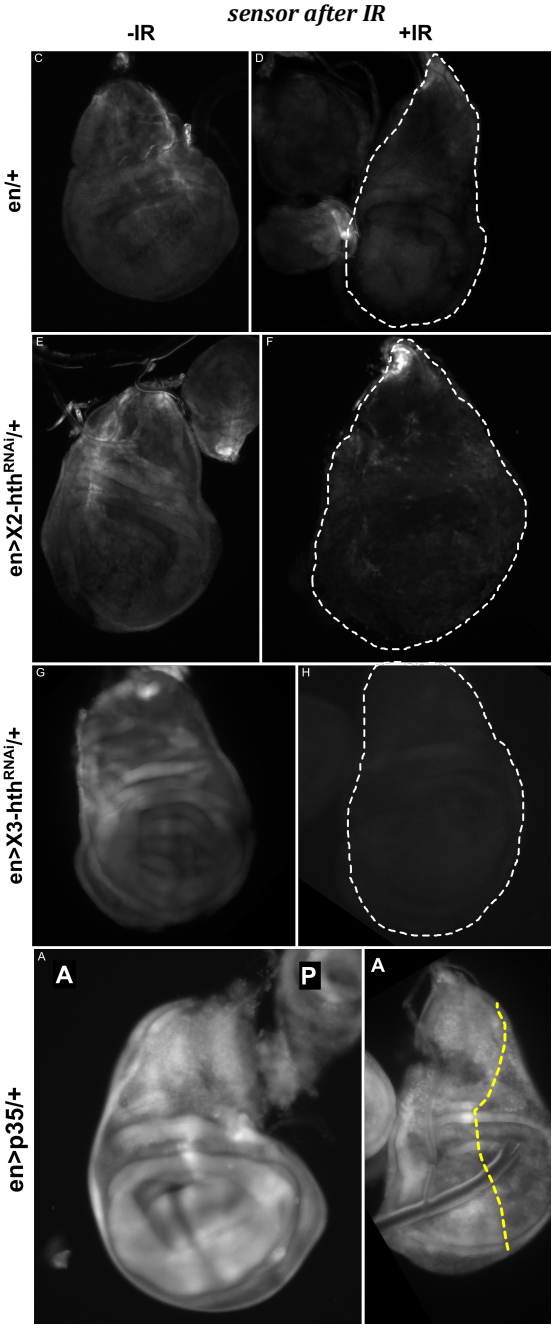

Figure 3B: Targeted knockdown of hth fails to modify ban expression. en>GAL4 was used to drive the expression hth RNAi (X2 and X3) in the posterior compartment of the wing disc. Flies expressing either the X2 or X3 hth-RNAi showed a uniform a reduction in anterior:posterior fluorescence following irradiation. Similar results were observed from 7-11 additional wing discs from two separate experiments. en>GAL4 was also used to drive the expression of the anti-apoptotic protein p35 (en>P35/+) in the posterior compartment of the wing disc (demarcated by yellow line). Inhibition of apoptosis resulted in increased EGFP expression in the posterior wing disc. Similar results were observed in 8 additional wing discs from two separate experiments. Embryos were collected for 24h at 18°C. 48h after the start of collection, flies were shifted from 18 °C to 29 °C for 72h. After 72h at 29°C, flies were treated with 4000R of IR and imaged 24h after irradiation. Images were processed identically for direct comparison of –IR to +IR group per genotype.

Figure 3C: ***Quantification of Fig. 3A GFP intensity***

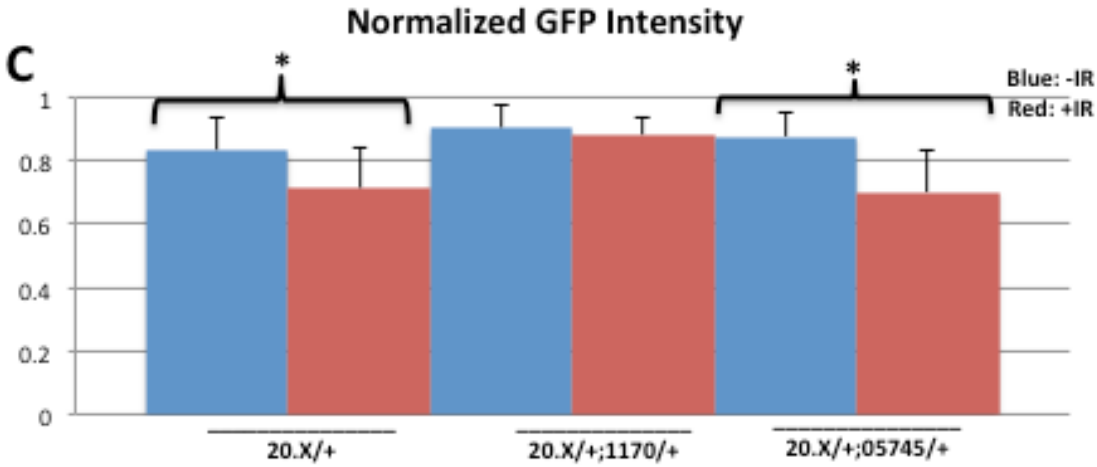

Fig. 3C: Quantification of figure 3A. ban sensor heterozygotes (20.X/+) and hth05745 heterozygotes (20.X showed a significant (*) reduction in fluorescence following irradiation (p<0.005 and p<0.006 respectively heterozygotes (20.X;11170/+) failed to show a significant change in EGFP expression following irradiatio together with figure 3A and 3B, these data indicate that ban expression is not reliant on hth in the wing in intensity values were normalized to highest value from un-irradiated discs. N=12-21 wing discs per genoty from at least two separate experiments. Two-tailed student T test was used to determine statistical significa mean fluorescence.

Homothorax affects wing disc growth following irradiation

The inhibition of *hth* in the posterior wing disc has been shown to result in cell non-autonomous overgrowth of the wing blade at the expense of the wing hinge. That is to say, adult *hth*$^{-}$ wing tissues have a wing phenotype in which there is an overgrown wing blade and no wing hinge (Casares and Mann 2000). Here it is shown that *hth* induced overgrowth is exacerbated by exposure to IR.

An *en*-GAL4 driver was used to co-express *hth*^{RNAi} (X2) and GFP in the posterior compartment of the wing disc. Following a 72h *hth* knockdown, larvae were exposed to 4000R of x-ray radiation. Flies were then allowed to recover at 25°C and discs were dissected/imaged 24h, 48h, and 72h after irradiation. The ratio between the size of the posterior:anterior compartment of the wing disc was used to quantify overgrowths. Though both -IR and +IR larvae showed irregular wing disc morphology, flies treated with radiation had larger overgrowths compared to their -IR counterparts (Fig. 4).

Figure 4A: ***IR exacerbates hth-induced overgrowths***

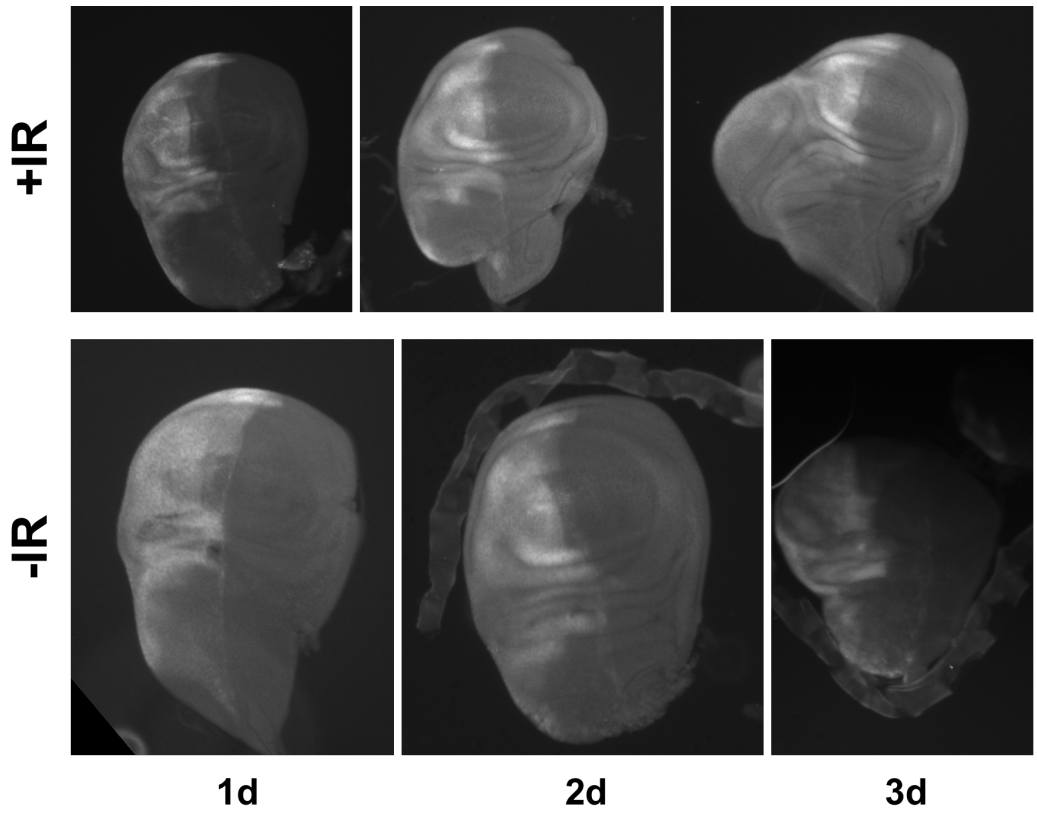

Figure 4A: Overlay of images of GFP and fluorescently labeled engrailed antibody from en>gfp/UAS-X2hth^{RNAi}/ wing discs. 1d, 2d, 3d refers to days after radiation

Figure 4B: ***Quantification of hth induced overgrowths***

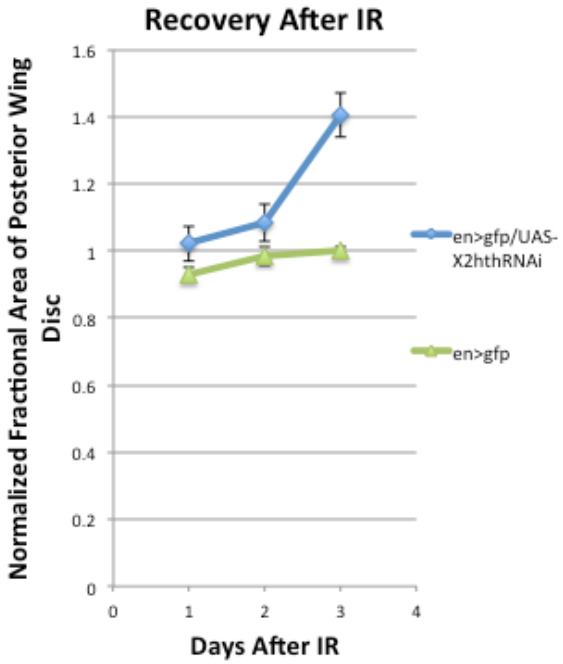

Figure 4B: Quantification of posterior wing disc normalized to -IR controls. N=10-20 wing discs per genotype per condition from two separate experiments.

Figure 4C: ***Experimental timeline***

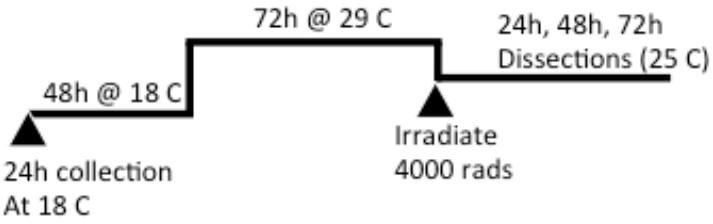

Figure 4C: Data collection followed proceeding timeline: 24h egg collection at 18°C, 48h growth at 18°C, shifted to 29°C for 72h to induce RNAi, irradiated at 25°C, and allowed to recover at 25°C until dissections at 24h, 48h, and 72h.

Preliminary data indicates Homothorax attenuates the Mahakali Effect

To address the role of *hth* in the Mahakali Effect, larvae heterozygous for the hypomorphic hth^{05745} allele used a GAL4-*UAS* system to express a dsRNA against *dE2F1* from a patched (*ptc)* promoter (henceforth referred to as PE3). Repression of the pro-mitotic gene, *dE2F1,* results in cell-autonomous apoptosis (Neufield et al. 1998). Subsequently, PE3 expressed in the *ptc* domain results in a stripe of apoptotic cells along the anterior-posterior wing compartment boundary (Bilak et al. 2014).

Consistent with previous findings, it was observed that irradiated larvae that had previously expressed PE3 had resistance to apoptosis from IR. The "PE3 (-GAL4)" larvae served as negative control as they did not express PE3 and subsequently failed show a protective effect. Again, Mahakali protection was found to be most profound in the anterior compartment of wing disc (Fig. 5). This allowed to posterior wing disc to serve as an internal control. The mean fluorescence intensity of caspase stain was measured in the anterior wing pouch and normalized to the posterior pouch as a marker for protection conferred via the Mahakali Effect. PE3/+ larvae were found have a normalized fluorescence intensity of 0.80 (s.d. ± 0.05). PE3/+;$ban^{\Delta 1}$/+ larvae were found to have a mean normalized intensity of 0.92 (s.d. ± 0.04) and PE3/+;hth^{05745}/+ larvae were found to have mean intensity of 0.96 (s.d. ± 0.05). From these measurements it is concluded that there was a statistically significant increase in fluorescence in the PE3/+;$ban^{\Delta 1}$/+ and PE3/+;hth^{05745}

Figure 5: ***hth attenuates the Mahakali Effect***

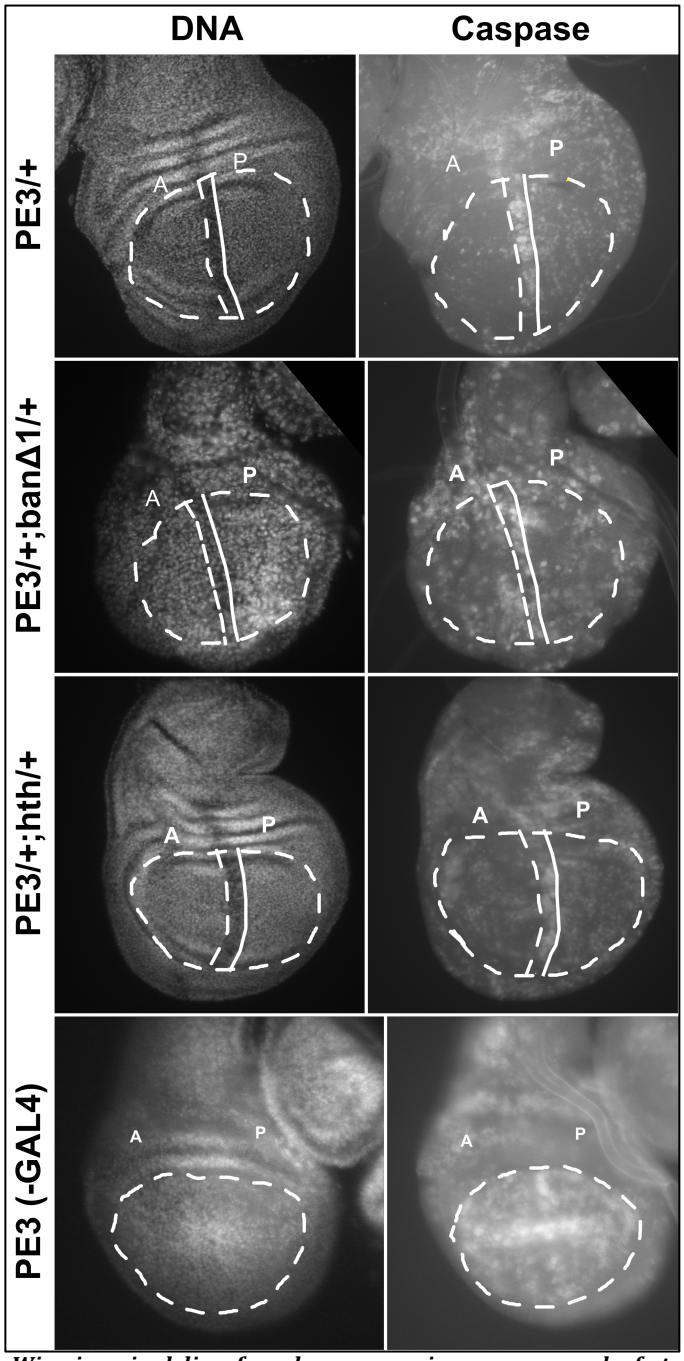

Figure 6: Wing imaginal discs from larvae carrying one copy each of ptc4-GAL4 and UAS-dsRNA against dE2F1 were fixed/stained for cleaved DCP-1 4h after irradiation with 4000R of IR. DNA stained images were used to locate the pouch (within the dashed line), the A/P boundary (solid vertical line) and the ptc domain (between vertical lines). The fluorescence intensity in the pouch was quantified as a marker for apoptosis. hth=hth^{05745}.

larvae compared to the PE3/+ control ($p<0.005$). This indicates that each of these groups had more cell death compared to the PE3/+ control. Examining the images of these discs reveals that PE3/+; $ban^{\Delta 1}$/+ and PE3/+;hth^{05745} larvae had markedly reduced protection from apoptosis in the anterior compartment of the wing disc. This increase in cell death in the anterior wing disc represents a reduction in protection from the Mahakali Effect. However, it should be noted that this experiment has been conducted once and yielded an N=5-10 discs per genotype. Currently this experiment is being repeated to ensure reproducibility and generate a larger sample size.

Discussion

Genetic Interaction Between *Homothorax* and *bantam*

The aim of this research was to identify genes involved in the regulation of *ban* expression. To approach this topic, a forward screen was conducted to look for *ban* phenotypic modifiers. Specifically, synergistic pupal lethality was used as a surrogate marker for genetic interaction with *ban*. Pupal lethality was an especially useful marker for two reasons. Firstly, it provided a binary phenotype that could easily be used to compare flies of disparate genetic backgrounds. Secondly, it revealed genetic combinations that were amenable to further investigation. Since flies that die as pupa necessarily survived through third instar, a means of investigating the consequences of genetic interaction is provided through the examination of limb and organ primordia.

Of the 161 genetic combinations screened, *hth* was identified as being able to reproducibly sensitize *ban* mutants to ionizing radiation (Fig. 1). This interaction was observed in two distinct *hth* and *ban* alleles. It was also noted that the interaction between *hth* and *ban* resulted in a diminished rate of pupation, indicating the animals were dying as early as the larval stage. This was especially pronounced when $ban^{\Delta 1}$ was crossed to *hth.* It was seen that irradiated $ban^{\Delta 1}/hth^{7637}$ larvae had 10% pupation (s.d. ± 7%), while hth^{7637}/+ larvae pupated 74% of the time (s.d. ± 14%), and $ban^{\Delta 1}$/+ larvae pupated 66% of the time (s.d. ± 13%). However given that the majority of un-irradiated *ban/hth* larvae that did pupate, also eclosed (and irradiated *ban/hth* did not), synthetic lethality in *ban/hth* larvae is concluded to be radiation dependent. It should also be noted that a reduction in *hth* alone did not result in an increased sensitivity to radiation (Fig. S2). Together, these data indicate that *hth* and *ban* are necessary but not individually

sufficient for the radiation sensitivity observed in Figure 1. It is also likely that this sensitivity responds to *ban* gene dosage.

The $ban^{\Delta 1}$ allele deletes the genetic locus for *ban* while ban^{1170} is generated from a transposable element insertion that interrupts a regulatory region of *ban.* Given this difference between alleles, it is probable that flies heterozygous for $ban^{\Delta 1}$ have less *ban* expression than flies heterozygous for ban^{1170} (Hipfner et al. 2002). The results observed in Fig. 1B reflect this disparity. The majority of irradiated $ban^{\Delta 1}/hth^{05745}$ larvae died before pupating while the majority of ban^{1170}/hth^{05745} larvae died as pupa. This indicates that ban^{1770} larvae had a marginally better response to radiation than $ban^{\Delta 1}$ larvae in a *hth* deficient background. However, $ban^{1170}/+$ and $ban^{\Delta 1}/+$ larvae were not observed to have significantly different rates of eclosion following irradiation (Fig. 1). Interestingly, this indicates that *hth* intensifies the distinction between these two *ban* alleles.

Radiation sensitivity is not the result of increased apoptosis

Given that *ban* has a known anti-apoptotic function and is up-regulated following exposure to IR, it was suspected that *hth/ban* flies might experience increased apoptosis following irradiation (Jaklevic et al. 2008). However, as shown in Figure 2, *hth* failed to modify apoptosis in the wing disc of *ban/+* flies. From this result it was concluded that apoptosis alone is unlikely to be responsible for *ban/hth* synthetic lethality. But it cannot be ruled out that apoptosis in additional organs is intensified by *ban/hth.* For example, *hth* in the eye imaginal disc is known to regulate *ban* expression (Peng et al. 2009). Consequently, it is likely that *ban* deficient eye discs would be hypersensitive to radiation. However, given the fact that eyeless mutant flies can still eclose from their pupal case (Halder et al. 1995), it would be surprising if apoptosis confined to the eye disc prevented eclosion. Ultimately, a more comprehensive investigation of cell death in imaginal discs could address their individual importance for eclosion.

Homothorax does not regulate *ban* activity in the wing disc

In accordance with findings made by Jaklevic et al. 2008, here it shown that *ban* sensor EGFP expression is diminished after exposure to IR (Fig. 3A and 3B). If *hth* were regulating *ban* activity, it would be expected that discs deficient in *hth* would retain EGFP expression following

irradiation. However, Figure 3 presents two lines of evidence that indicate *ban* activity is not dependent on *hth.* One, hth^{05745}/+ larvae have reduced EGFP expression that is similar to 20.X/+ (*ban* sensor only) larvae following irradiation. Two, *en*>GAL4/UAS-hth^{RNAi} larvae failed to retain EGFP expression in the posterior compartment following irradiation. Future investigation could corroborate this evidence by directly measuring GFP via western blot.

It was also observed that both irradiated and un-irradiated *en*>GAL4/UAS-hth^{RNAi} larvae had markedly reduced EGFP expression compared to 20.X/+;hth^{05745}/+ counterparts. This is likely due to increased apoptotic cell death resulting from the elimination of *hth* in the posterior compartment of the wing disc (Fig. S3). Given *ban's* ability to be induced in a cell non-autonomous manner following apoptosis, localized cell death in the posterior compartment of the wing disc has the potential evoke *ban* expression in the entire wing disc (Bilak et al. 2014). However, the elevated levels of apoptosis resulting from hth^{RNAi} were not found to affect pupal eclosion (Fig. S2).

Figure 3 indicates that *hth* likely has an indirect interaction with *ban*. Considering the fact that *ban* is known to have a complex regulatory region (insertions over 10kb from the promoter result in a *ban* phenotype), this was not an unlikely result (Bernnecke et al. 2003). Interestingly, miRNA levels of *ban* are unchanged following exposure to ionizing radiation, despite an increase in *ban* activity (Jaklevic et al. 2008). Subsequently, it is likely that there are *ban* activators. It is possible that *hth* only plays a permissive role in regulating *ban* activation. It is conceivably that repeated cell death consumes *ban* or a *ban* activating protein at a rate that cannot be replenished by a diminished *hth* allele. If this scenario were true, it would explain why *hth* is associated with an attenuated Mahakali Effect but failed to change *ban* activity after a single apoptotic event. To further investigate this hypothesis, *ban* sensor expression should be measured in *hth* deficient flies that have been exposed to multiple doses of IR.

Apoptosis in *homothorax* and *ban* result in contrasting phenotypes

Flies harboring mutations in *ban* have been shown to grow smaller wing discs and have a diminished ability to mitigate cell death following irradiation compared to wild-type flies (Fig. 5) (Jaklevic et al. 2008). The elimination of *hth* via RNAi also results in increased apoptosis following radiation (Fig S2). However, unlike the elimination of *ban,* which reduces wing disc size*,* the elimination of *hth* results in wing disc overgrowths (Casares and Mann 2000) (Fig. 4).

Also unlike *ban,* the increase in apoptosis from the elimination of *hth* does not correlate significantly with a reduction in eclosion after irradiation (Jaklevic et al. 2008 and Figure S1). In this regard, the phenotypes observed by the individual elimination of either *ban* or *hth* are in stark contrast to one another. This indicates that apoptosis alone is not indicative of organismal radiation sensitivity.

One factor other than apoptosis that likely plays a role in radiation sensitivity is the ability to recover from cell death. Unlike *ban, hth* knockdown via RNAi resulted in aberrant cell migration. Cells usually confined to the anterior compartment of the wing disc were observed to migrate from the hinge into the posterior compartment (Fig. S3). This aberrant cell migration was heightened by exposure to IR. The wing hinge, which is naturally resistant to apoptosis, contains a population of cells that contribute to regeneration following irradiation (Verghese and Su 2016). In normal wing disc regeneration, cells that migrate from the hinge change fate to form a homogenous population with the tissues they regenerate (Tamori et al. 2016). However, the elimination of *hth* appears to disrupt the cell-signaling boundary that spatially confines certain cell populations within the wing disc. Given that when *hth* is exposed to IR, tissues experience overgrowths (Fig. 4), aberrant cell migration (Fig S3), and diminished protection from the Mahakali Effect (Fig. 5), it is concluded that *hth* plays a role in ensuring proper recovery from exposure to radiation. Ultimately, it is speculated that some combination of cell death (from *ban* dysfunction) and aberrant recovery (from *hth* dysfunction) results in the synthetic lethality observed in *ban/hth* pupa following irradiation.

Future Aims

The mechanistic link between *ban* and *hth* has yet to be absolutely established. The individual disruption of each gene results in phenotypes that have the potential to explain the observed radiation sensitivity. However, a synergistic connection (other than the phenotype observed in the forward genetic screen) has yet to be positively identified. Subsequently, future investigations will be aimed at establishing this link. Experiments measuring *hth* induced overgrowth and aberrant cell migration need to completed in *ban* deficient background. It would also be valuable to repeat the caspase staining experiments in leg imaginal discs, given their role in eclosion from the pupal case. Lastly, the relationship between *hth* and *ban* needs to be examined with regards to repeated inductions of cell death.

Supplemental Figures

Figure S1A: ***hth does not modify radiation sensitivity***

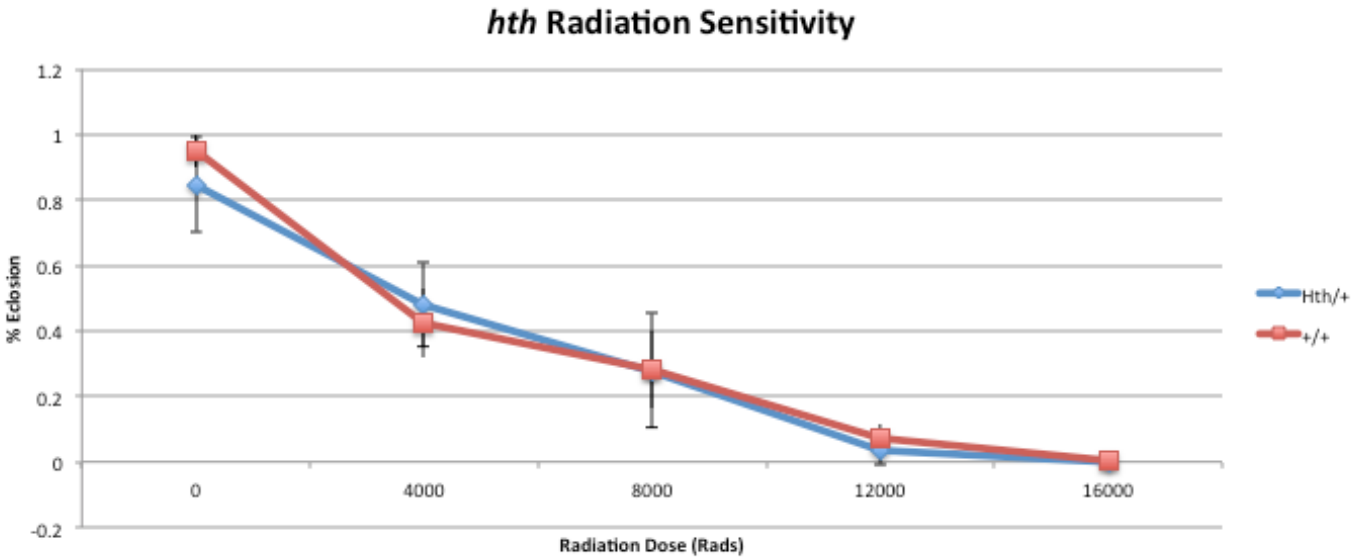

Figure S2A: Dose response to radiation of hth (hth7637/+) vs. wild type (w1118) larvae. All doses fail to produce statistically significant difference between both groups. N=252-387 pupa from two separate experiments.

Figure S1B: ***hth^{RNAi} does not sensitize pupa to IR***

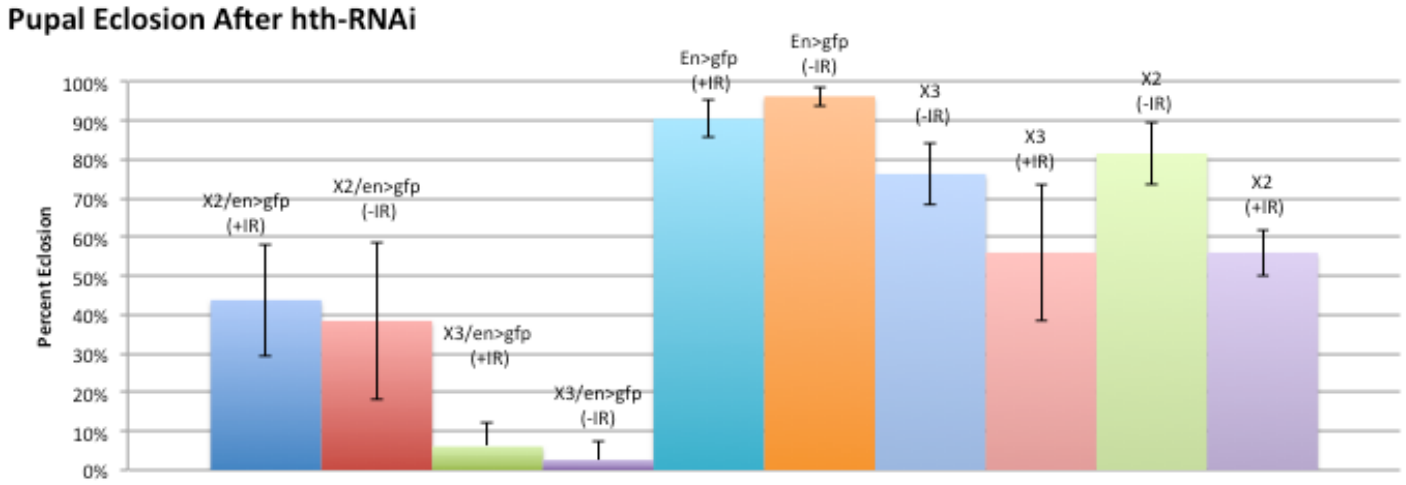

Figure S2B: Percent eclosion from flies treated with hth^{RNAi} (X2 and X3) and controls. Flies en>GAL4 used to co-expressed hth^{RNAi} as well as GFP from an engrailed promoter. Subsequently flies containing just UAS-hth^{RNAi} or en>GAL4 (en>GFP), failed to express hth^{RNAi}. Expression of hth^{RNAi} failed to sensitize larvae to radiation. N=91-388 pupa from at least two separate experiments. Experimental timeline is as described Fig. 3, eclosion measured 10 days after irradiation.

Figure S2: ***Apoptosis and cell migration following hth^{RNAi}***

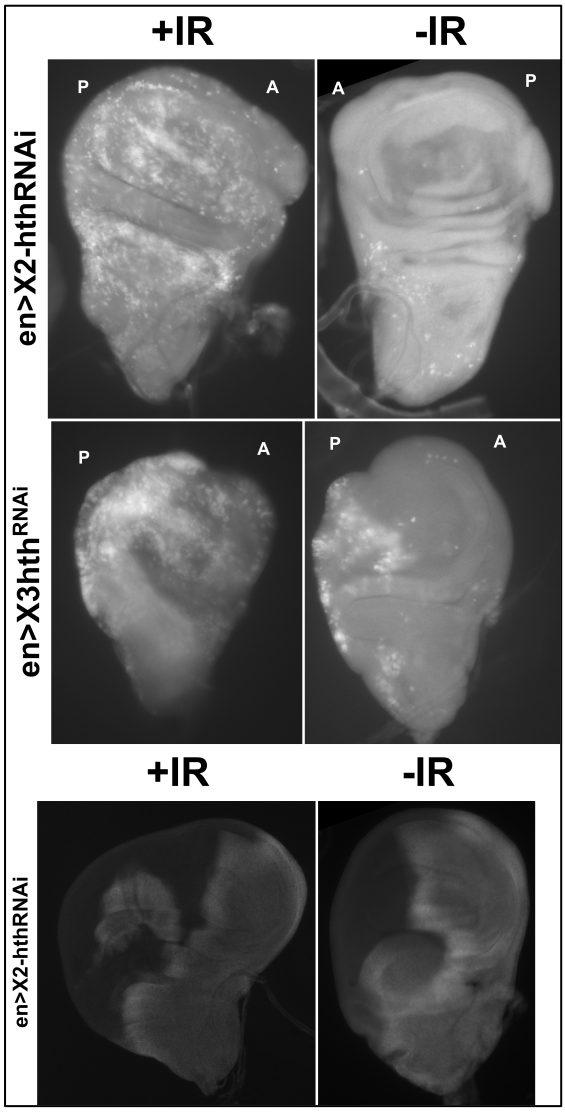

Figure S3: (Top) Images of wing discs stained for cleaved caspase (DCP-1) after exposure to 4000R of radiation and expression of hth^{RNAi} (X2 and X3). Note increased apoptosis in posterior compartment of wing disc (labeled with "P"), where hth^{RNAi} was expressed. Similar results observed in 5-8 additional wing discs per condition per genotype. Experimental conditions followed Fig. 3, discs fixed/stained 4h after irradiation. (Bottom) Images of discs fluorescently labeled with antibody against ci. Ci is normally confined to anterior compartment of wing disc but can be observed migrating into posterior compartment from wing hinge after expression of hth^{RNAi}. Experimental conditions followed Fig 3., discs fixed/stained 72h after irradiation. Primary antibody diluted in NGS at 1:500.

Fig S3: Deficiencies screened in Fig. 1

Bloomington Stock #	Genotype	Bloomington Stock #	Genotype
7413	Df(3R)BSC43, st[1] ca[1]/TM2, p[p]	7726	w[1118]; Df(3R)Exel6259, P{w[+mC]=XP-U}Exel6259/TM6B, Tb[1]
7535	w[1118]; Df(2R)Exel6053, P{w[+mC]=XP-U}Exel6053/CyO	7730	w[1118]; Df(3R)Exel6263, P{w[+mC]=XP-U}Exel6263/TM6B, Tb[1]
7565	w[1118]; Df(3L)Exel6086, P{w[+mC]=XP-U}Exel6086/TM6B, Tb[1]	7731	w[1118]; Df(3R)Exel6264, P{w[+mC]=XP-U}Exel6264/TM6B, Tb[+]
7591	w[1118]; Df(3L)Exel6112, P{w[+mC]=XP-U}Exel6112/TM6B, Tb[1]	7732	w[1118]; Df(3R)Exel6265, P{w[+mC]=XP-U}Exel6265/TM6B, Tb[1]
7594	w[1118]; Df(3L)Exel6115, P{w[+mC]=XP-U}Exel6115/TM6B, Tb[1]	7734	w[1118]; Df(3R)Exel6267, P{w[+mC]=XP-U}Exel6267/TM6B, Tb[1]
7601	w[1118]; Df(3L)Exel6122, P{w[+mC]=XP-U}Exel6122/TM6B, Tb[1]	7736	w[1118]; Df(3R)Exel6269, P{w[+mC]=XP-U}Exel6269/TM6B, Tb[1]
7619	w[1118]; Df(3R)Exel6140, P{w[+mC]=XP-U}Exel6140/TM6B, Tb[1]	7737	w[1118]; Df(3R)Exel6270, P{w[+mC]=XP-U}Exel6270/TM6B, Tb[1]
7620	w[1118]; Df(3R)Exel6141, P{w[+mC]=XP-U}Exel6141/TM6B, Tb[1]	7739	w[1118]; Df(3R)Exel6272, P{w[+mC]=XP-U}Exel6272/TM6B, Tb[1]
7621	w[1118]; Df(3R)Exel6142, P{w[+mC]=XP-U}Exel6142/TM6B, Tb[1]	7740	w[1118]; Df(3R)Exel6273, P{w[+mC]=XP-U}Exel6273/TM6B, Tb[1]
7622	w[1118]; Df(3R)Exel6143, P{w[+mC]=XP-U}Exel6143/TM6B, Tb[1]	7741	w[1118]; Df(3R)Exel6274, P{w[+mC]=XP-U}Exel6274/TM6B, Tb[1]
7623	w[1118]; Df(3R)Exel6144, P{w[+mC]=XP-U}Exel6144/TM6B, Tb[1]	7742	w[1118]; Df(3R)Exel6275, P{w[+mC]=XP-U}Exel6275/TM6B, Tb[1]
7625	w[1118]; Df(3R)Exel6146, P{w[+mC]=XP-U}Exel6146/TM6B, Tb[1]	7746	w[1118]; Df(3R)Exel6280, P{w[+mC]=XP-U}Exel6280/TM6B, Tb[1]
7626	w[1118]; Df(3R)Exel6147, P{w[+mC]=XP-U}Exel6147/TM6B, Tb[1]	7752	w[1118]; Df(3R)Exel6288, P{w[+mC]=XP-U}Exel6288/TM6B, Tb[1]
7627	w[1118]; Df(3R)Exel6148, P{w[+mC]=XP-U}Exel6148/TM6B, Tb[1]	7917	w[1118]; Df(3R)Exel9020/TM6B, Tb[1]
7628	w[1118]; Df(3R)Exel6149, P{w[+mC]=XP-U}Exel6149/TM6B, Tb[1]	7918	w[1118]; Df(3R)Exel8194/TM6B, Tb[1]
7629	w[1118]; Df(3R)Exel6150, P{w[+mC]=XP-U}Exel6150/TM6B, Tb[1]	7919	w[1118]; Df(3R)Exel7379/TM6B, Tb[1]
7630	w[1118]; Df(3R)Exel6151, P{w[+mC]=XP-U}Exel6151/TM6B, Tb[1]	7925	w[1118]; Df(3L)Exel9028, PBac{w[+mC]=RB5.WH5}Exel9028
7631	w[1118]; Df(3R)Exel6152, P{w[+mC]=XP-U}Exel6152/TM6B, Tb[1]	7931	w[1118]; Df(3R)Exel7315/TM6B, Tb[1]
7632	w[1118]; Df(3R)Exel6153, P{w[+mC]=XP-U}Exel6153/TM6B, Tb[1]	7932	w[1118]; Df(3R)Exel7317/TM6B, Tb[1]
7633	w[1118]; Df(3R)Exel6154, P{w[+mC]=XP-U}Exel6154/TM6B, Tb[1]	7948	w[1118]; Df(3R)Exel7357/TM6B, Tb[1]
7634	w[1118]; Df(3R)Exel6155, P{w[+mC]=XP-U}Exel6155/TM6B, Tb[1]	7951	w[1118]; Df(3R)Exel9029, PBac{w[+mC]=RB3.WH3}Exel9029

7635	w[1118]; Df(3R)Exel6156, P{w[+mC]=XP-U}Exel6156/TM6B, Tb[1]	7952	w[1118]; Df(3R)Exel7283/TM6B, Tb[1]
7636	w[1118]; Df(3R)Exel6157, P{w[+mC]=XP-U}Exel6157/TM6B, Tb[1]	7953	w[1118]; Df(3R)Exel7284/TM6B, Tb[1]
7637	w[1118]; Df(3R)Exel6158, P{w[+mC]=XP-U}Exel6158/TM6B, Tb[1]	7954	w[1118]; Df(3R)Exel8143/TM6B, Tb[1]
7638	w[1118]; Df(3R)Exel6159, P{w[+mC]=XP-U}Exel6159/TM6B, Tb[1]	7955	w[1118]; Df(3R)Exel9036, PBac{w[+mC]=WHr}Exel9036/TM6B, Tb[1]
7639	w[1118]; Df(3R)Exel6160, P{w[+mC]=XP-U}Exel6160/TM6B, Tb[1]	7956	w[1118]; Df(3R)Exel7305/TM6B, Tb[1]
7640	w[1118]; Df(3R)Exel6161, P{w[+mC]=XP-U}Exel6161/TM6B, Tb[+]	7957	w[1118]; Df(3R)Exel7306/TM6B, Tb[1]
7641	w[1118]; Df(3R)Exel6162, P{w[+mC]=XP-U}Exel6162/TM6B, Tb[1	7958	w[1118]; Df(3R)Exel8152/TM6B, Tb[1]
7642	w[1118]; Df(3R)Exel6163, P{w[+mC]=XP-U}Exel6163/TM6B, Tb[1]	7959	w[1118]; Df(3R)Exel7308/TM6B, Tb[1]
7643	w[1118]; Df(3R)Exel6164, P{w[+mC]=XP-U}Exel6164/TM6B, Tb[1]	7960	w[1118]; Df(3R)Exel7309/TM6B, Tb[1]
7644	w[1118]; Df(3R)Exel6165, P{w[+mC]=XP-U}Exel6165/TM6B, Tb[1]	7961	w[1118]; Df(3R)Exel8154/TM6B, Tb[1]
7645	w[1118]; Df(3R)Exel6166, P{w[+mC]=XP-U}Exel6166/TM6B, Tb[1]	7962	w[1118]; Df(3R)Exel9018/TM6B, Tb[1]
7646	w[1118]; Df(3R)Exel6167, P{w[+mC]=XP-U}Exel6167/TM6B, Tb[1]	7963	w[1118]; Df(3R)Exel8153/TM6B, Tb[1]
7647	w[1118]; Df(3R)Exel6168, P{w[+mC]=XP-U}Exel6168/TM6B, Tb[1]	7964	w[1118]; Df(3R)Exel9019/TM6B, Tb[1]
7648	w[1118]; Df(3R)Exel6169, P{w[+mC]=XP-U}Exel6169/TM6B, Tb[1]	7965	w[1118]; Df(3R)Exel7310/TM6B, Tb[1]
7649	w[1118]; Df(3R)Exel6170, P{w[+mC]=XP-U}Exel6170/TM6B, Tb[1]	7966	w[1118]; Df(3R)Exel7312/TM6B, Tb[1]
7650	w[1118]; Df(3R)Exel6171, P{w[+mC]=XP-U}Exel6171/TM6B, Tb[1]	7967	w[1118]; Df(3R)Exel8155/TM6B, Tb[1]
7651	w[1118]; Df(3R)Exel6172, P{w[+mC]=XP-U}Exel6172/TM6B, Tb[1]	7968	w[1118]; Df(3R)Exel7313/TM6B, Tb[1]
7652	w[1118]; Df(3R)Exel6173, P{w[+mC]=XP-U}Exel6173/TM6B, Tb[1]	7969	w[1118]; Df(3R)Exel7314/TM6B, Tb[1]
7653	w[1118]; Df(3R)Exel6174, P{w[+mC]=XP-U}Exel6174/TM6B, Tb[1]	7970	w[1118]; Df(3R)Exel7316/TM6B, Tb[1]
7655	w[1118]; Df(3R)Exel6176, P{w[+mC]=XP-U}Exel6176/TM6B, Tb[1]	7972	w[1118]; Df(3R)Exel7318/TM6B, Tb[1]
7658	w[1118]; Df(3R)Exel6179, P{w[+mC]=XP-U}Exel6179/TM6B, Tb[1]	7974	w[1118]; Df(3R)Exel8158/TM6B, Tb[1]
7659	w[1118]; Df(3R)Exel6180, P{w[+mC]=XP-U}Exel6180/TM6B, Tb[1]	7975	w[1118]; Df(3R)Exel7320/TM6B, Tb[1]
7660	w[1118]; Df(3R)Exel6181, P{w[+mC]=XP-U}Exel6181/TM6B,	7976	w[1118]; Df(3R)Exel8159/TM6B, Tb[1]

	Tb[1]		
7661	w[1118]; Df(3R)Exel6182, P{w[+mC]=XP-U}Exel6182/TM6B, Tb[1]	7977	w[1118]; Df(3R)Exel7321/TM6B, Tb[1]
7662	w[1118]; Df(3R)Exel6183, repo[*] P{w[+mC]=XP-U}Exel6183/TM6B, Tb[1]	7980	w[1118]; Df(3R)Exel7326/TM6B, Tb[1]
7663	w[1118]; Df(3R)Exel6184, P{w[+mC]=XP-U}Exel6184/TM6B, Tb[1]	7981	w[1118]; Df(3R)Exel8162/TM6B, Tb[1]
7664	w[1118]; Df(3R)Exel6185, P{w[+mC]=XP-U}Exel6185/TM6B, Tb[1]	7982	w[1118]; Df(3R)Exel7327/TM6B, Tb[1]
7665	w[1118]; Df(3R)Exel6186, P{w[+mC]=XP-U}Exel6186/TM6B, Tb[1]	7983	w[1118]; Df(3R)Exel7328/TM6B, Tb[+]
7666	w[1118]; Df(3R)Exel6187, P{w[+mC]=XP-U}Exel6187/TM6B, Tb[1]	7984	w[1118]; Df(3R)Exel7329/TM6B, Tb[1]
7667	w[1118]; Df(3R)Exel6188, P{w[+mC]=XP-U}Exel6188/TM6B, Tb[1]	7985	w[1118]; Df(3R)Exel7330/TM6B, Tb[1]
7668	w[1118]; Df(3R)Exel6189, P{w[+mC]=XP-U}Exel6189/TM6B, Tb[1]	7987	w[1118]; Df(3R)Exel8163/TM6B, Tb[1]
7669	w[1118]; Df(3R)Exel6190, P{w[+mC]=XP-U}Exel6190/TM6B, Tb[1]	7989	w[1118]; Df(3R)Exel9030, PBac{w[+mC]=RB5.WH5}Exel9030/TM6B, Tb[1]
7670	w[1118]; Df(3R)Exel6191, P{w[+mC]=XP-U}Exel6191/TM6B, Tb[1]	7990	w[1118]; Df(3R)Exel9012/TM6B, Tb[1]
7671	w[1118]; Df(3R)Exel6192, P{w[+mC]=XP-U}Exel6192/TM6B, Tb[1]	7991	w[1118]; Df(3R)Exel9013/TM6B, Tb[1]
7672	w[1118]; Df(3R)Exel6193, P{w[+mC]=XP-U}Exel6193/TM6B, Tb[1]	7992	w[1118]; Df(3R)Exel9014/TM6B, Tb[1]
7673	w[1118]; Df(3R)Exel6194, P{w[+mC]=XP-U}Exel6194/TM6B, Tb[1]	7993	w[1118]; Df(3R)Exel8178/TM6B, Tb[+]
7674	w[1118]; Df(3R)Exel6195, P{w[+mC]=XP-U}Exel6195/TM6B, Tb[1]	7994	w[1118]; Df(3R)Exel9056/TM6B, Tb[1]
7676	w[1118]; Df(3R)Exel6197, P{w[+mC]=XP-U}Exel6197/TM6B, Tb[1]	7997	w[1118]; Df(3R)Exel7378/TM6B, Tb[1]
7677	w[1118]; Df(3R)Exel6198, P{w[+mC]=XP-U}Exel6198/TM6B, Tb[1]	8104	w[1118]; Df(3R)ED5780, P{w[+mW.Scer\FRT.hs3]=3'.RS5+3.3'}ED5780/TM2
7678	w[1118]; Df(3R)Exel6199, P{w[+mC]=XP-U}Exel6199/TM6B, Tb[1]	8681	w[1118]; Df(3R)ED5196, P{w[+mW.Scer\FRT.hs3]=3'.RS5+3.3'}ED5196/TM6C, cu[1] Sb[1]
7679	w[1118]; Df(3R)Exel6200, P{w[+mC]=XP-U}Exel6200/TM6B, Tb[1]	8685	w[1118]; Df(3R)ED7665, P{w[+mW.Scer\FRT.hs3]=3'.RS5+3.3'}ED7665/TM6C, cu[1] Sb[1]
7680	w[1118]; Df(3R)Exel6201, P{w[+mC]=XP-U}Exel6201/TM6B, Tb[1]	8965	w[1118]; Df(3R)ED5156, P{w[+mW.Scer\FRT.hs3]=3'.RS5+3.3'}ED5156/TM6C, cu[1] Sb[1]
7681	w[1118]; Df(3R)Exel6202, P{w[+mC]=XP-U}Exel6202/TM6B, Tb[1]	8967	w[1118]; Df(3R)ED5147, P{w[+mW.Scer\FRT.hs3]=3'.RS5+3.3'}ED5147/TM6C, cu[1] Sb[1]
7682	w[1118]; Df(3R)Exel6203, P{w[+mC]=XP-U}Exel6203/TM6B, Tb[+]	9075	w[1118]; Df(3R)ED5020, P{w[+mW.Scer\FRT.hs3]=3'.RS5+3.3'}ED5020/TM6C, cu[1] Sb[1]
7683	w[1118]; Df(3R)Exel6204, P{w[+mC]=XP-U}Exel6204/TM6B, Tb[1]	9090	w[1118]; Df(3R)ED5644, P{w[+mW.Scer\FRT.hs3]=3'.RS5+3.3'}ED5644/TM6C, cu[1] Sb[1]

7684	w[1118]; Df(3R)Exel6205, P{w[+mC]=XP-U}Exel6205/TM6B, Tb[1]	9152	w[1118]; Df(3R)ED5705, P{w[+mW.Scer\FRT.hs3]=3'.RS5+3.3'}ED5705/TM3, Ser[1]
7686	w[1118]; Df(3R)Exel6208, P{w[+mC]=XP-U}Exel6208/TM6B, Tb[1]	9198	w[1118]; Df(3R)ED5142, P{w[+mW.Scer\FRT.hs3]=3'.RS5+3.3'}ED5142/TM6C, cu[1] Sb[1]
7687	w[1118]; Df(3R)Exel6209, P{w[+mC]=XP-U}Exel6209/TM6B, Tb[1]	24142	w[1118]; Df(3R)ED6346, P{w[+mW.Scer\FRT.hs3]=3'.RS5+3.3'}ED6346/TM6C, cu[1] Sb[1]
7688	w[1118]; Df(3R)Exel6210, P{w[+mC]=XP-U}Exel6210/TM6B, Tb[1]	24971	w[1118]; Df(3R)BSC467/TM6C, Sb[1] cu[1]
7689	w[1118]; Df(3R)Exel6211, P{w[+mC]=XP-U}Exel6211/TM6B, Tb[1]	25005	w[1118]; Df(3R)BSC501/TM6C, Sb[1] cu[1]
7690	w[1118]; Df(3R)Exel6212, P{w[+mC]=XP-U}Exel6212/TM6B, Tb[1]	25011	w[1118]; Df(3R)BSC507/TM6C, Sb[1] cu[1]
7691	w[1118]; Df(3R)Exel6213, P{w[+mC]=XP-U}Exel6213/TM6B, Tb[1]	25050	w[1118]; Df(3R)BSC522/TM6C, Sb[1]
7692	w[1118]; Df(3R)Exel6214, P{w[+mC]=XP-U}Exel6214/TM6B, Tb[1]	25075	w[1118]; Df(3R)BSC547/TM6C, Sb[1]
7693	w[1118]; Df(3R)Exel6215, P{w[+mC]=XP-U}Exel6215/TM6B, Tb[1]	25390	w[1118]; Df(3R)BSC567/TM6C, Sb[1]
7694	w[1118]; Df(3R)Exel6216, P{w[+mC]=XP-U}Exel6216/TM6B, Tb[1]	26280	l(3)76BDh[1] red[1] e[4]/TM6B, Sb[1] Tb[1] ca[1]
7695	w[1118]; Df(3R)Exel6217, P{w[+mC]=XP-U}Exel6217/TM6B, Tb[1]	26836	w[1118]; Df(3R)BSC738/TM6C, Sb[1] cu[1]
7696	w[1118]; Df(3R)Exel6218, P{w[+mC]=XP-U}Exel6218/TM6B, Tb[1]	26837	w[1118]; Df(3R)BSC739/TM6C, Sb[1] cu[1]
		26847	w[1118]; Df(3R)BSC749, P+PBac{w[+mC]=XP3.WH3}BSC749/TM6C, Sb[1] cu[1]
		27365	w[1118]; Df(3R)BSC793/TM6C, Sb[1] cu[1]
		27919	w[1118]; Df(3R)BSC846/TM6C, Sb[1] cu[1]
		37742	w[1118]; Df(3R)PS2/TM6B, Tb[1]

Acknowledgements

This project would not have been possible without the tremendous support and feedback I have received from all members of the Su Lab. I would like to thank Dr. Shilpi Verghese for teaching me techniques necessary for *Drosophila* research and for helping me troubleshoot my experiments. I would also like to thank Dr. Tin Tin Su for her continued support and mentorship throughout this project. Finally, I would like to thank Dr. Christy Fillman and Dr. Rebecca Safran for taking time out of their schedule to be part of this thesis process.

Works Cited

1. Aagaard, L. & Rossi, J. J. RNAi therapeutics: Principles, prospects and challenges. *Adv. Drug Deliv. Rev.* **59,** 75–86 (2007).

2. Alberto del Valle Rodríguez, D. D. & C. D. Power tools for gene expression and clonal analysis in Drosophila. *Nat.* **9,** (2012).

3. Aldaz, S. & Escudero, L. M. Imaginal discs. *Curr. Biol.* **20,** R429–R431 (2010).

4. Ayala-Camargo, A. *et al.* JAK/STAT signaling is required for hinge growth and patterning in the Drosophila wing disc. *Dev. Biol.* **382,** 413–26 (2013).

5. Bartel, D. P. MicroRNAs: Target Recognition and Regulatory Functions. *Cell* **136,** 215–233 (2009).

6. Beira, J. V & Paro, R. The legacy of Drosophila imaginal discs. *Chromosoma* **125,** 573–92 (2016).

7. Bilak, A. & Su, T. T. Regulation of Drosophila melanogaster pro-apoptotic gene hid. *Apoptosis* **14,** 943–9 (2009).

8. Bilak, A., Uyetake, L. & Su, T. T. No Title. **10,** e1004220 (2014).

9. Bonnet, D. & Dick, J. E. Human acute myeloid leukemia is organized as a hierarchy that originates from a primitive hematopoietic cell. *Nat. Med.* **3,** 730–737 (1997).

10. Brennecke, J., Hipfner, D. R., Stark, A., Russell, R. B. & Cohen, S. M. bantam encodes a developmentally regulated microRNA that controls cell proliferation and regulates the proapoptotic gene hid in Drosophila. *Cell* **113,** 25–36 (2003).

11. Brown, J. M. & Wouters, B. G. Apoptosis, p53, and Tumor Cell Sensitivity to Anticancer Agents. *CANCER Res.* **59,** 1391–1399 (1999).

12. Calin, G. A. & Croce, C. M. MicroRNA signatures in human cancers. *Nat. Rev. Cancer* **6,** 857–866 (2006).

13. Casares, F. & Mann, R. S. A dual role for homothorax in inhibiting wing blade development and specifying proximal wing identities in Drosophila. *Development* **127,** 1499–508 (2000).

14. Casso, D., Âs, F.-A., Ârez-Weber, R. & Kornberg, T. B. GFP-tagged balancer chromosomes for Drosophila melanogaster. at <https://pdfs.semanticscholar.org/ee99/695e015697b883dc5b6b099b29a331012d3b.pdf>

15. Chow, A. Y. No Title. *Nat. Educ.* **3,** 7 (2010).

16. Collins, C. T. & Hess, J. L. Role of HOXA9 in leukemia: dysregulation, cofactors and essential targets. *Oncogene* **35,** 1090–1098 (2016).

17. Corish, P. & Tyler-Smith, C. Attenuation of green fluorescent protein half-life in mammalian cells. *Protein Eng.* **12,** 1035–40 (1999).

18. Duffy, J. B. GAL4 system indrosophila: A fly geneticist's swiss army knife. *genesis* **34,** 1–15 (2002).

19. Faber, J. *et al*. HOXA9 is required for survival in human MLL-rearranged acute leukemias. *Blood* **113,** 2375–2385 (2009).

20. Fan, Y. *et al*. Dual roles of Drosophila p53 in cell death and cell differentiation. *Cell Death Differ*. **17,** 912–921 (2010).

21. George A. Calin and Carlo M. Croce. MicroRNA signatures in human cancers. *Nature* **6,** (2006).

22. Grzeschik, N. A., Amin, N., Secombe, J., Brumby, A. M. & Richardson, H. E. Abnormalities in cell proliferation and apico-basal cell polarity are separable in Drosophila lgl mutant clones in the developing eye. *Dev. Biol*. **311,** 106–23 (2007).

23. Halder, G., Callaerts, P. & Gehring, W. J. Induction of ectopic eyes by targeted expression of the eyeless gene in Drosophila. *Science* **267,** 1788–92 (1995).

24. Hipfner, D. R., Weigmann, K. & Cohen, S. M. The bantam Gene Regulates Drosophila Growth. at <https://www.ncbi.nlm.nih.gov/pmc/articles/PMC1462212/pdf/12196398.pdf>

25. Huang, J., Zhou, W., Watson, A. M., Jan, Y.-N. & Hong, Y. Efficient ends-out gene targeting in Drosophila. *Genetics* **180,** 703–7 (2008).

26. Jackson, S. P. & Bartek, J. The DNA-damage response in human biology and disease. *Nature* **461,** 1071–1078 (2009).

27. Julia Winter, S. J. S. K. & Richard. Gregory and Sven Diederichs. Many roads to maturity: microRNA biogenesis pathways and their regulation. *Nature* **11,** (2009).

28. Kim, K. & McBride, W. H. Modifying radiation damage. *Curr. Drug Targets* **11,** 1352–65 (2010).

29. Kornbluth, S. Apoptosis in Drosophila: neither fish nor fowl (nor man, nor worm). *J. Cell Sci*. **118,** 1779–1787 (2005).

30. Krivtsov, A. V. *et al*. Transformation from committed progenitor to leukaemia stem cell initiated by MLL–AF9. *Nature* **442,** 818–822 (2006).

31. Kroon, E. *et al*. Hoxa9 transforms primary bone marrow cells through specific collaboration with Meis1a but not Pbx1b. *EMBO J*. **17,** 3714–25 (1998).

32. Kwak, P. B., Iwasaki, S. & Tomari, Y. The microRNA pathway and cancer. *Cancer Sci*. **101,** 2309–2315 (2010).

33. Lam, J. K. W., Chow, M. Y. T., Zhang, Y. & Leung, S. W. S. siRNA Versus miRNA as Therapeutics for Gene Silencing. *Mol. Ther. - Nucleic Acids* **4,** e252 (2015).

34. Lee, H. *et al*. Drosophila RB proteins repress differentiation-specific genes via two different mechanisms. *Mol. Cell. Biol*. **30,** 2563–77 (2010).

35. Lee, R. C., Feinbaum, R. L. & Ambros, V. The C. elegans heterochronic gene lin-4 encodes small RNAs with antisense complementarity to lin-14. *Cell* **75,** 843–854 (1993).

36. Levine, A. J. & Oren, M. The first 30 years of p53: growing ever more complex. *Nat. Rev. Cancer* **9,** 749–58 (2009).

37. Lloyd, T. E. & Taylor, J. P. Flightless flies: Drosophila models of neuromuscular disease. *Annals of the New York Academy of Sciences* **1184,** (2010).

38. Longley, D. & Johnston, P. Molecular mechanisms of drug resistance. *J. Pathol.* **205,** 275–292 (2005).

39. Lowe, S. W., Schmitt, E. M., Smith, S. W., Osborne, B. a & Jacks, T. P53 Is Required for Radiation-Induced Apoptosis in Mouse Thymocytes. *Nature* **362,** 847–849 (1993).

40. Matthew J. Wolf, H. A. R. Drosophila, Genetic Screens, and Cardiac Function. *Am. Hear. Assoc.* **109,** 794–806 (2011).

41. Nahmad, M., Stathopoulos, A., Nakano, Y., Stark, D. & Neave, B. Dynamic Interpretation of Hedgehog Signaling in the Drosophila Wing Disc. *PLoS Biol.* **7,** e1000202 (2009).

42. Neufeld, T. P., Flor, A., De La Cruz, A., Johnston, L. A. & Edgar, B. A. Coordination of Growth and Cell Division in the Drosophila Wing. *Cell* **93,** 1183–1193 (1998).

43. Papatheodorou, I., Petrovs, R. & Thornton, J. M. Comparison of the mammalian insulin signalling pathway to invertebrates in the context of FOXO-mediated ageing. *Bioinformatics* **30,** 2999–3003 (2014).

44. Pawlik, T. M. & Keyomarsi, K. Role of cell cycle in mediating sensitivity to radiotherapy. *Int. J. Radiat. Oncol.* **59,** 928–942 (2004).

45. Peng, H. W., Slattery, M. & Mann, R. S. Transcription factor choice in the Hippo signaling pathway: homothorax and yorkie regulation of the microRNA bantam in the progenitor domain of the Drosophila eye imaginal disc. *Genes Dev.* **23,** 2307–19 (2009).

46. Ronald L. Johnson, J. K. G. and M. P. S. patched overexpression alters wing disc size and pattern: transcriptional and post-transcriptional effects on hedgehog targets. *Development* **121,** 4161–4170 (1995).

47. Ronald L. Johnson, J. K. G. and M. P. S. patched overexpression alters wing disc size and pattern: transcriptional and post-transcriptional effects on hedgehog targets. *Dev.* **121,** 4161–4170 (1995).

48. Ryoo, H. D., Marty, T., Casares, F., Affolter, M. & Mann, R. S. Regulation of Hox target genes by a DNA bound Homothorax/Hox/Extradenticle complex. *Development* **126,** 5137–48 (1999).

49. Salvesen, G. S. & Duckett, C. S. Apoptosis: IAP proteins: blocking the road to death's door. *Nat. Rev. Mol. Cell Biol.* **3,** 401–410 (2002).

50. Shklover, Jeny, Levy-Adam, F. & Kurant, E. The role of Drosophila TNF Eiger in developmental and damage-induced neuronal apoptosis. *FEBS Lett.* **589,** 871–879 (2015).

51. Shklover, J., Levy-Adam, F. & Kurant, E. in 297–334 (2015). doi:10.1016/bs.ctdb.2015.07.024

52. Siegel, R. L., Miller, K. D. & Jemal, A. Cancer statistics, 2015. *CA. Cancer J. Clin.* **65,** 5–29 (2015).

53. Simón, R., Aparicio, R., Housden, B. E., Bray, S. & Busturia, A. Drosophila p53 controls Notch expression and balances apoptosis and proliferation. *Apoptosis* **19,** 1430–1443 (2014).

54. Steller, H. Regulation of apoptosis in Drosophila. *Cell Death Differ*. **15,** 1132–1138 (2008).

55. Tamori, Y. *et al*. Epithelial Tumors Originate in Tumor Hotspots, a Tissue-Intrinsic Microenvironment. *PLOS Biol*. **14,** e1002537 (2016).

56. Therond, P. *et al*. Molecular organisation and expression pattern of the segment polarity gene fused of Drosophila melanogaster. *Mech. Dev*. **44,** 65–80 (1993).

57. Tin Su, T. Non-autonomous consequences of cell death and other perks of being metazoan. *AIMS Genet*. **2,** 54–69 (2015).

58. Verghese, S. *et al*. Drosophila Wnt and STAT Define Apoptosis-Resistant Epithelial Cells for Tissue Regeneration after Irradiation. *PLOS Biol*. **14,** e1002536 (2016).

59. Vitulo, N. *et al*. Characterization and evolution of the cell cycle-associated mob domain-containing proteins in eukaryotes. *Evol. Bioinform. Online* **3,** 121–58 (2007).

60. Vogelstein, B. *et al*. Cancer genome landscapes. *Science* **339,** 1546–58 (2013).

61. Wichmann, A., Jaklevic, B. & Su, T. T. Ionizing radiation induces caspase-dependent but Chk2- and p53-independent cell death in Drosophila melanogaster. *Proc. Natl. Acad. Sci. U. S. A*. **103,** 9952–7 (2006).

62. Wolf, M. J. & Rockman, H. A. Drosophila, Genetic Screens, and Cardiac Function. *Circ. Res*. **109,** 794–806 (2011).

63. Yeo, S. L. *et al*. On the functional overlap between two Drosophila POU homeo domain genes and the cell fate specification of a CNS neural precursor. *Genes Dev*. **9,** 1223–36 (1995).